THE PENNSYLVANIA STATE UNIVERSITY
SCHREYER HONORS COLLEGE

DEPARTMENT OF ENGINEERING SCIENCE AND MECHANICS

# DATA ASSIMILATION OF GLUCOSE DYNAMICS FOR THE NEURO-ICU

KENNETH HALL
SPRING 2017

A thesis
submitted in partial fulfillment
of the requirements
for a baccalaureate degree
in Engineering Science
with honors in Engineering Science

Reviewed and approved* by the following:

Bruce Gluckman
Professor of Engineering Science
Thesis Supervisor

Clifford Lissenden
Professor of Engineering Science
Honors Adviser

Judith A. Todd
Department Head
Engineering Science and Mechanics

*Signatures are on file in the Schreyer Honors College and Engineering Science and Mechanics Office.

# Abstract

Measurements of plasma glucose are used to make decisions about insulin delivery in diabetic patients, make judgments about the effectiveness of diabetes treatment, and set feeding levels for incapacitated patients in the Intensive Care Unit. Glucose/insulin dynamics are highly nonlinear and oscillatory even at constant input, which complicates therapy decisions by necessitating an understanding of both current and future system behavior. This paper presents an application of data assimilation to the study of glucose/insulin dynamics. A state estimate is propagated forward in time by using an Unscented Kalman Filter to fit a mathematical representation of glucose and insulin dynamics to serial glucose and feeding data. This approach enables a prediction of near-future dynamics, as well as the reconstruction of unmeasured variables including interstitial insulin, plasma insulin, or exogenous glucose delivery.

# Table of Contents

# List of Figures

# List of Tables

# Acknowledgments

Felix, qui potuit rerum cognoscere causas: Fortunate are those able to know the causes of things. Thank you, Dr. Bruce Gluckman, for helping a willing pupil to see a little bit further. I aspire to your clarity of understanding and depth of knowledge. Thank you, Fatemeh Bahari, for getting me started with Matlab Code for the Unscented Kalman Filter. Thank you to Dr. David Albers of Columbia University, for sharing your insight on the Sturis glucose/insulin model.

# Dedication

*For Nicki*

# Chapter 1
# Introduction

## 1.1 Motivation

Glucose/insulin dynamics involves complex nonlinear feedback mechanisms between food input, blood and peripheral levels of glucose and insulin, metabolic draw, and organ regulatory functions. Although blood glucose and insulin levels can be measured, the relationship between food consumption and the time-course of glucose input is uncertain.

Accurate prediction and control of blood glucose levels creates the potential for a variety of new clinical health-care solutions such as model-based meal guidance for type II diabetics, and feeding control for comatose patients.

Type II diabetic patients need a tool which can predict the effect of each meal choice on their future glucose levels. Insulin resistance, the hallmark of type II diabetes, inhibits the action of insulin in transporting glucose from the blood to interstitial tissue. Chronically high levels of blood glucose can cause neuropathy and nephropathy resulting in fatigue, changes in vision and urination, poor wound healing, and Alzheimer's disease, and a range of other severe complications. Patients with type II diabetes will benefit from glucose tracking, prediction and reconstruction to aid in making meal decisions, and to track changes in their degree of insulin resistance over time.

In the Neuro-ICU, blood glucose levels must be externally managed for comatose patients. Caretakers manage blood glucose by providing feeding through a tube, at a continuous rate. If a patient's blood glucose is too high, the feeding rate may be decreased or insulin supplementation may be warranted. The goal of intervention is to maintain a normal level of blood glucose. However, glucose and insulin oscillate vigorously and continuously in healthy people. Due to the nonlinearity of the glucose/insulin system, it is impossible to know what action (if any) should be taken from a single measurement of blood glucose. Continuous tracking and estimation of all system variables is necessary to predict future glucose dynamics and enable effective intervention when a problem is indicated.

## 1.2 Hypothesis

Data assimilation can be used with a basic mathematical model of glucose/insulin dynamics to create useful predictions of future glucose behavior, and to reconstruct the dynamics of food consumption or other unmeasured variables from measurements of blood glucose levels.

## 1.3 Application Context

### 1.3.1 Continuously Measured Glucose in Healthy Subjects

Two nondiabetic subjects recorded blood glucose levels in five minute intervals for thirty days. The measurement device was a Dexcom G4 Platinum, and several gaps in data collection occur when the sensor was removed and refreshed. In addition to continuously monitored blood glucose, both subjects periodically reported finger-prick glucose measurements and calories consumed. Meal nutritional information and calories were recorded and estimated by the subjects, and then later evaluated by experts using photographs.

Subject one recorded 10,645 glucose measurements and 175 meals over a span of 38 days. Subject two recorded 7,722 glucose measurements and 73 meals over a span of 31 days.

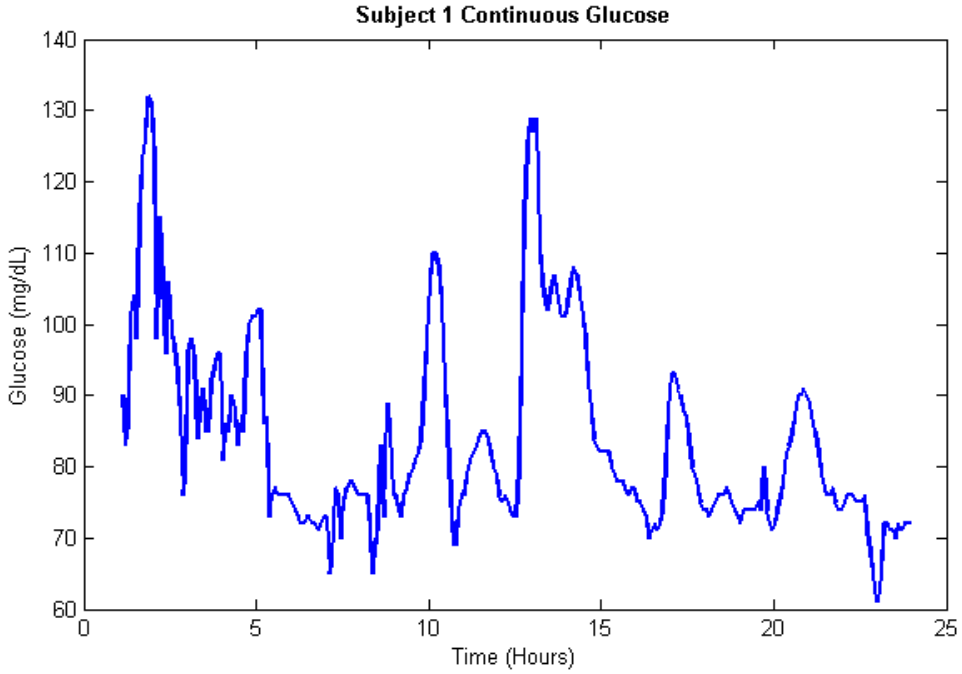


**Figure 1.1.** One day of continuously monitored blood glucose from Subject 1

During this day, subject 1 had three meals of 162 calories at 9.4 hours, 357 calories at 12.2 hours, and 451 calories at 19.7 hours. There are clear peaks in the subject's blood glucose following each of these meals. However, it is clear that the subject's blood glucose level is highly variable throughout the day. For instance, there is a peak in blood glucose at 21 hours which is of similar magnitude to that at 19.7 hours despite the fact that the subject did not report consuming a meal at that time.

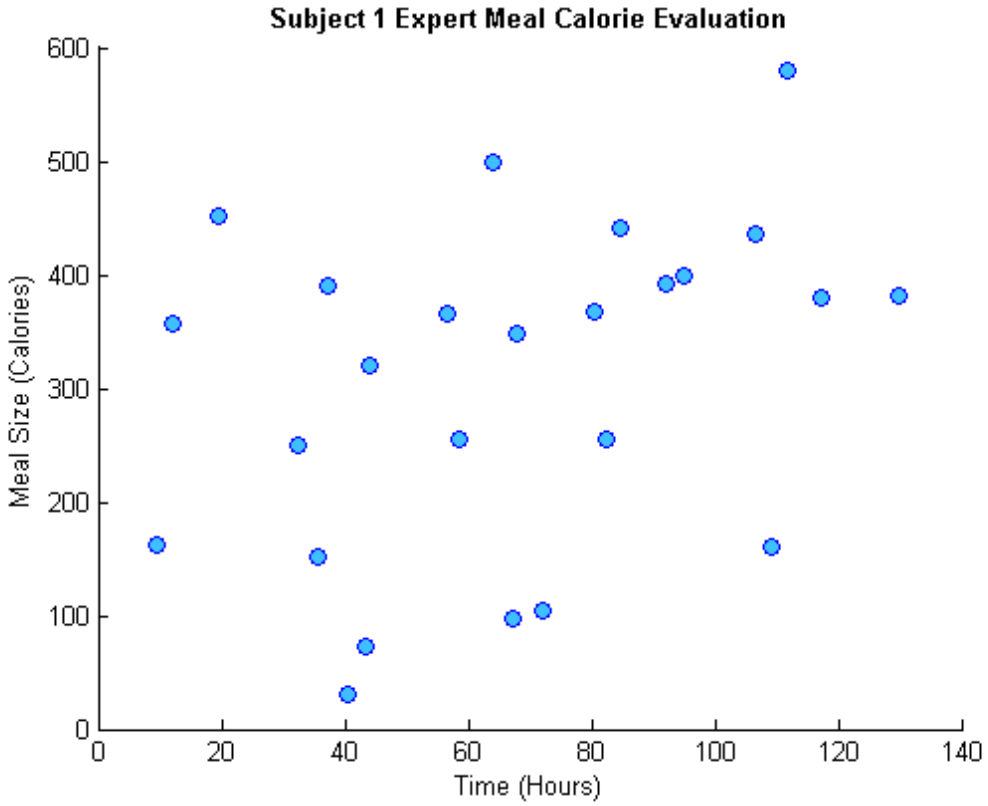


**Figure 1.2.** Expert evaluation of calorie content for 140 hours of subject 1 meals

Subject 1 consumes 4 to 5 meals each day, with meal size varying from 31 calories to 1219 calories. Using calorie information to analyze blood glucose is challenging, since food type has a dramatic impact on the time delay between eating and the change in blood glucose. Certain types of carbohydrates have a rapid effect on blood glucose, beginning within minutes of consumption. However, protein is digested more slowly and might continue to affect blood glucose levels for many hours.

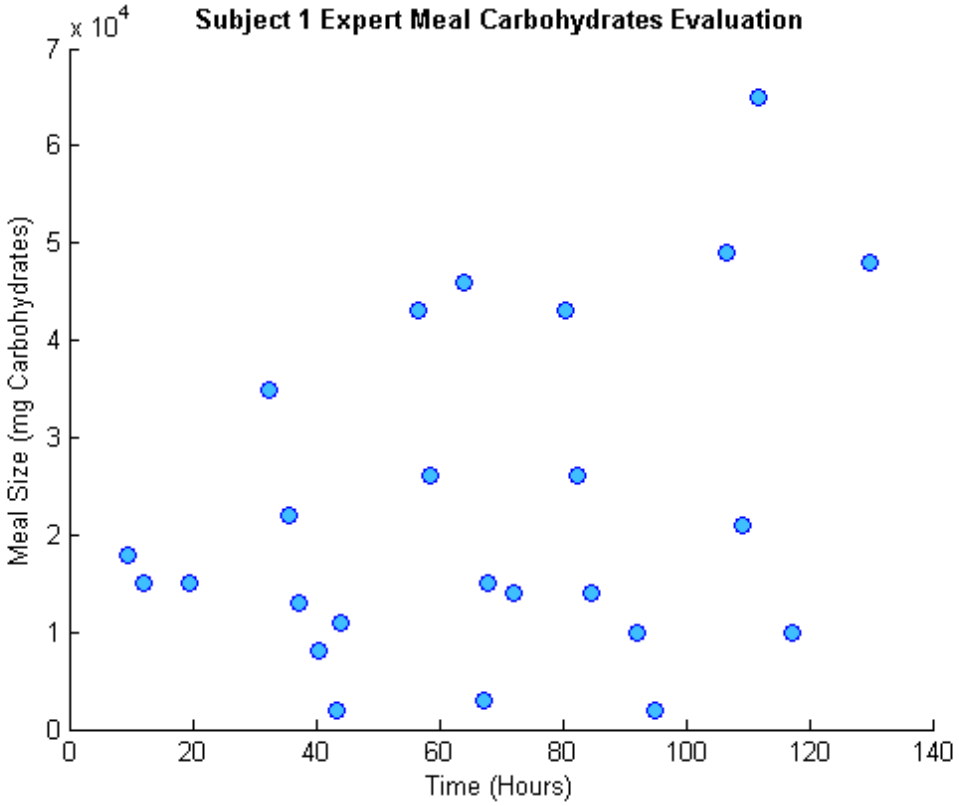


**Figure 1.3.** Expert evaluation of carbohydrate content for 140 hours of subject 1 meals

Some meals appear relatively larger or smaller when measured by carbohydrate content. Meals that have high calories but low carbohydrate content will cause unpredictable error when used to predict future glucose behavior. In chapter 5, glucose prediction will be compared for two cases:

1. Meal size measured in carbohydrate content is used as feeding
2. Meal size measured in calorie content is used as feeding

### 1.3.2 Continuous Feeding in Neuro-ICU Patients

This work draws from a set of Electronic Health Record data for 599 patients in the Neuro-ICU. Patients in the Neuro-ICU are fed at a continuous rate which is occasionally altered to regulate blood glucose level. Measurements of blood glucose are taken one or more times each day, and the rate of feeding may be adjusted more or less frequently than glucose is measured. The length of time over which measurements occur as well as the measurement frequency and number vary widely from one patient to the next. Patient 596 has only 46 glucose measurements and 4 feeding rate adjustments over a duration of 7.5 days, whereas patient 311 has 1446 glucose measurements and 4438 feeding rate adjustments over a duration of 339 days. The best patient data for use with data assimilation methods will have a high measurement frequency of glucose, and a low number of feeding rate adjustments.

The measurements of glucose in Neuro-ICU data are sparse compared to the 5-minute interval of measurement in the continuously monitored dataset. Patient 311 had 14 measurements of glucose over a 24-hour period, displayed in the figure above. Several hours pass between some measurements. What makes the Neuro-ICU data uniquely valuable is that patients undergo extended periods with continuous feeding. This is a situation which is unlikely to occur, even in dedicated continuous glucose monitoring patients.

Of all patients in the 599-person dataset, patient 311 has the highest number of

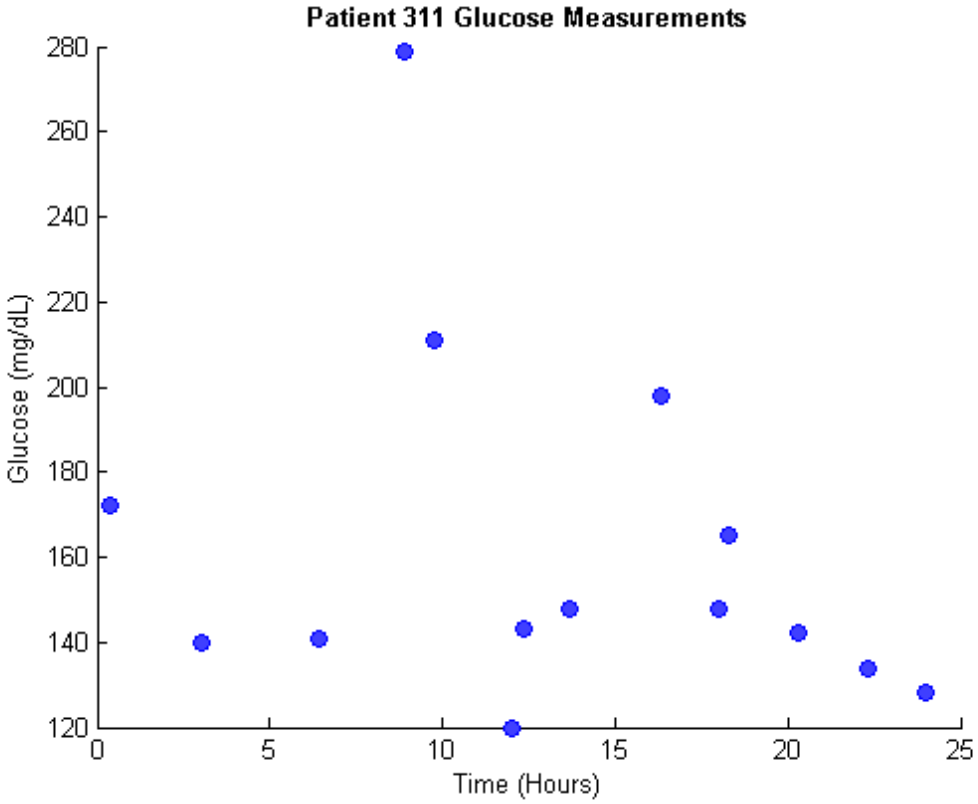


**Figure 1.4.** One day of blood glucose measurements from patient 311

adjustments to the feeding rate (4438 adjustments in total). In the figure above, the rate of feeding is adjusted 20 times over a 24-hour period. Clearly, something about this patient's condition required close monitoring of blood glucose levels and frequent intervention in the rate of feeding to control it.

## 1.4 Use of Data Assimilation

Two goals of this work are:

1. To reconstruct a patient's rate of feeding from measurements of blood glucose levels. Such reconstructions can be used to map the time-dependence of glucose absorption to the type and quantity of food consumed. Accurate reconstructions of food consumption provide evidence that the Sturis model is

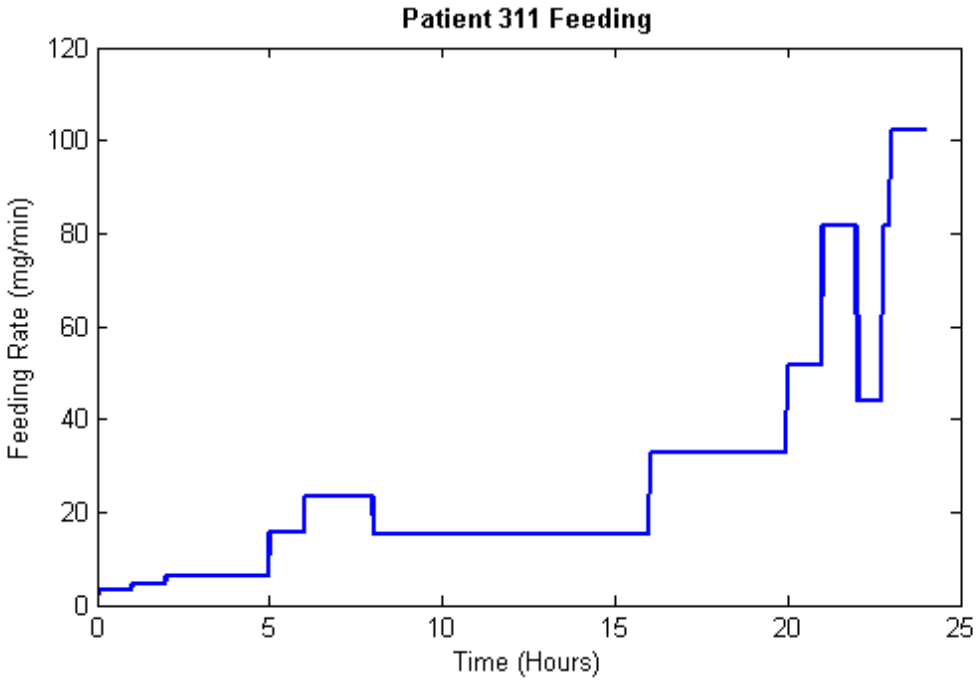


**Figure 1.5.** One day of feeding data for patient 311

an accurate and useful representation of the physical processes of glucose/insulin dynamics, and might therefore be suitable for projecting future glucose behavior.

2. To project future glucose dynamics when the feeding amount is known. One application is control system design for automatic glucose maintenance in comatose patients. Another use is for identifying safe meal content for type II diabetic patients who wish to maintain blood glucose levels within a set range.

The high glucose measurement frequency in the continuously monitored healthy patient dataset is advantageous for reconstruction of feeding as well as precise knowledge about the accuracy of glucose projections. However, the feeding information represents a challenge since calories consumed may behave unpredictably compared to continuous steady-state feeding. In the Electronic Health Record data from the Neuro-ICU, the rate of feeding is precisely known and is stepwise constant.

The low frequency of glucose measurement under-samples the ultradian oscillations of glucose and insulin. However, an advantage of this dataset is that the validity of feeding rate reconstructions is easily and precisely evaluated since the feeding rate is often constant for an extended length of time..

Feeding reconstruction and future glucose behavior projection for the continuously measured glucose dataset are presented in chapter 5. Success in feeding reconstruction and glucose projection on this dataset validate that the Sturis model accurately represents glucose/insulin dynamics. Feeing reconstruction and future glucose behavior projection are applied to the Electronic Health Record (Neuro-ICU) data in chapter 6.

# Chapter 2
# Modeling Glucose Dynamics

## 2.1 Glucose/Insulin Physiology

Glucose is a courier used to distribute digested food energy throughout the body. It travels in the circulatory system, and its concentration is regulated by the hormone insulin. The balance of glucose and insulin is regulated by multiple feedback mechanisms. Plasma glucose increases upon digestion of food, and by the release of glucose from the liver which follows primarily from the breakdown of glycogen. The amount of plasma glucose may decrease in two ways: 1) Insulin-independent utilization, such as in the brain. 2) Insulin-dependent utilization.

Insulin may exist in plasma, or at remote sites outside of the bloodstream; both types play an important role in maintaining dynamic equilibrium with glucose. The pancreas secretes insulin when plasma glucose reaches a high concentration. However, low plasma glucose stimulates the release of glucagon from the pancreas, which results in increased breakdown of glycogen in the liver. Plasma insulin is also lost continuously due to filtering by the kidneys and liver. Positive feedback between plasma insulin and plasma glucose is balanced by the effect of remote insulin, which is the insulin present in interstitial tissue. Remote insulin greatly increases the efficiency of glucose utilization through the recruitment of glucose carriers in the plasma membrane of interstitial cells. Remote insulin decreases

through degradation in muscle, and also through exchange with plasma insulin [3].

## 2.2 Rodbard Model

In 1989, two years prior to the publication of the Sturis model (used extensively in this work), a non-oscillating computational model of glucose/insulin dynamics was proposed by Rodbard et al [1]. Intended as a tool for doctors and diabetic patients, this model was developed with a first principles approach based upon a two-pool model of glucose and insulin. Instead of separating interstitial insulin into a separate basin, the model algorithmically "activates" plasma insulin.

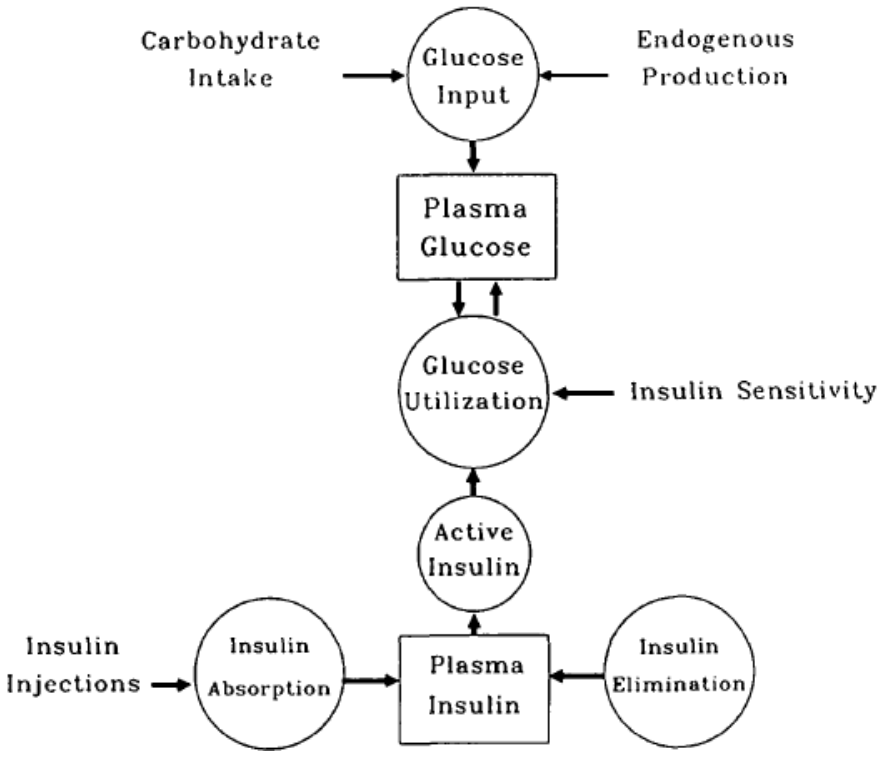


**Figure 2.1.** Schematic representation of Rodbard's model [1]

Rodbard's model fails to recreate some of the key experimental observations around which the Sturis model is constructed. The ultradian oscillations which characterize the normal behavior of the Sturis model are absent in Rodbard's. This

is consistent with the observation of Sturis et al. that the separation of insulin into two pools is necessary for ultradian oscillations to occur. Another notable difference is the failure to reproduce a delay between changes in plasma glucose and plasma insulin. In Rodbard's model, insulin injection produces notable glucose oscillations. However, there are no corresponding oscillations in the insulin profile. In the Sturis model, changes in plasma glucose always lead changes in plasma insulin by several minutes.

The shortcomings of Rodbard's model provide context for the desire to find an oscillatory glucose/insulin model which motivated the model developed in Sturis et al. Although not originally intended to be used in predicting single-patient glucose/insulin behavior, the Sturis model represents the underlying dynamics successfully enough to produce acceptable agreement with experimental data.

## 2.3 Sturis Model

### 2.3.1 Overview

Experimental observations of glucose and insulin in humans demonstrate oscillations on both short and long time scales. Seeking an explanation for this ultradian oscillatory behavior, Sturis et. al proposed a mathematical representation (Sturis model) of glucose dynamics which employs negative feedback loops between glucose and insulin to produce periodicity [2].

Observation of ultradian glucose oscillations in segmental pancreas transplant patients contraindicates nervous regulation of pancreatic insulin release. The unsuccessful search for an intrapancreatic ultradian pacemaker was a primary motivating factor behind the development of the Sturis model. By employing two insulin pools and one glucose pool with two feedback loops, the Sturis model is able to replicate ultradian oscillatory behavior consistent with three experimental observations:

1. Oscillations with constant amplitude at steady-state feeding

2. Damped oscillations following a short feeding pulse

3. Insulin oscillation which follows glucose behavior by 10-20 minutes [2].

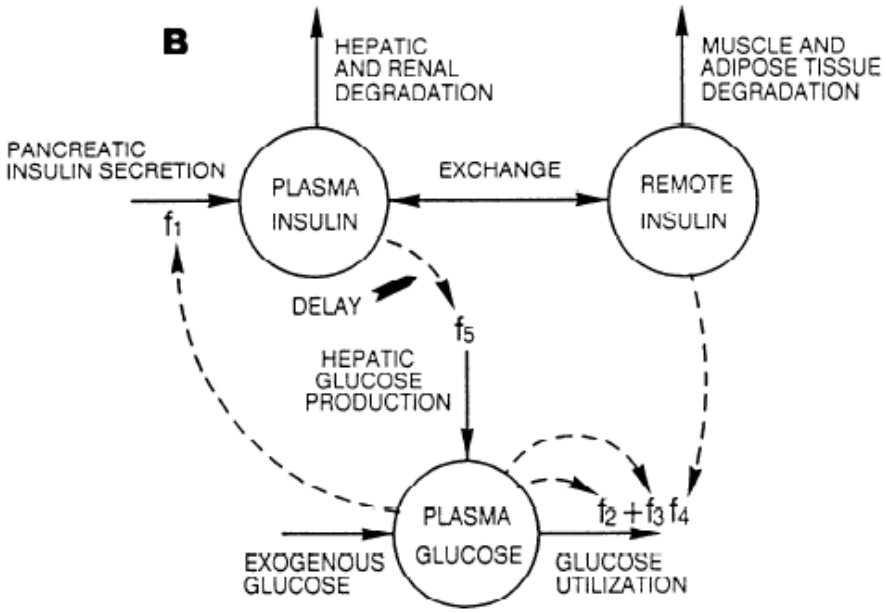


**Figure 2.2.** Diagram of Sturis Model [2]

### 2.3.2 Model Details

Insulin is separated into two separate pools: interstitial liquid insulin, and plasma insulin. Plasma glucose comprises a third pool. These three model pools are represented by three differential equations. Insulin dependent glucose release occurs with a 25 to 50-minute time delay, which is implemented as a three-stage linear filter (three equations).

Plasma Insulin Pool

$$\frac{dI_p}{dt} = f_1(G) - (\frac{I_p}{V_p} - \frac{I_i}{V_i})E - \frac{I_p}{t_p} \tag{2.1}$$

**Table 2.1.** Plasma Insulin Terms

| | |
|---|---|
| $f_1(G)$ | Glucose dependent production of plasma insulin |
| $(\frac{I_p}{V_p} - \frac{I_i}{V_i})E$ | Exchange of plasma insulin with remote (interstitial) insulin |
| $\frac{I_p}{t_p}$ | Decay of plasma insulin - removal by kidneys and liver |

Remote Insulin Pool

$$\frac{dI_i}{dt} = (\frac{I_p}{V_p} - \frac{I_i}{V_i})E - \frac{I_i}{t_i} \tag{2.2}$$

**Table 2.2.** Remote Insulin Terms

| | |
|---|---|
| $(\frac{I_p}{V_p} - \frac{I_i}{V_i})E$ | Exchange of plasma insulin with remote (interstitial) insulin |
| $\frac{I_i}{t_i}$ | Decay of remote insulin - degradation by fat |

Glucose Pool

$$\frac{dG}{dt} = f_4(h_3) + I_G(t) - f_2(G) - f_3(I_i)G \tag{2.3}$$

**Table 2.3.** Glucose Terms

| | |
|---|---|
| $f_4(h_3)$ | Insulin dependent glucose production |
| $I_G(t)$ | External glucose addition (feeding) |
| $f_2(G)$ | Insulin independent glucose utilization (brain) |
| $f_3(I_i)G$ | Insulin dependent glucose utilization (remote tissues) |

Linear Filter

$$t_d \frac{dh_1}{dt} = I_p - h_1 \tag{2.4}$$

$$t_d \frac{dh_2}{dt} = h_1 - h_2 \tag{2.5}$$

$$t_d \frac{dh_3}{dt} = h_2 - h_3 \tag{2.6}$$

This filter regulates the time delay in the release of glucose by the pancreas that is regulated by plasma insulin. The Sturis model recommends using at least three stages in the linear filter, as using too few stages can reduce the amplitude of ultradian oscillations.

Numerical Model Evaluation

The Sturis model does not have a known analytic solution, so numerical integration is the preferred method of use. Sturis et al. employed 6th order Runge-Kutta to produce the results in their paper [2].

### 2.3.3 Ultradian Oscillations

Model Structure

Two delays resulting in latent feedback loops drive ultradian oscillations.

1. Instantaneous plasma insulin affects glucose levels 25-50 minutes in the future [2]. Experiments show that in humans, approximately 36 minutes pass between an increase in insulin and the increase in glucose which follows it. The Sturis model implements this delay as a three-stage linear filter.

2. While plasma insulin production is an increasing function of plasma glucose, interstitial insulin (and not plasma insulin) affects glucose utilization. This results in an implicit delay in the Sturis model.

These two feedback mechanisms are necessary, but not sufficient, to produce ultradian oscillations. In their paper, Sturis et al. determine that condition (2)

from above is of interesting physiological significance, as it suggests that two insulin pools are a required assumption in producing the desired oscillatory behavior. This lends strength to their case against an intrapancreatic ultradian pacemaker.

Behavior of Dependency Functions ($f_1 - f_4$)

Crucial in determining the amplitude of ultradian oscillations is the shape of the functions $f_1 - f_4$.

**Table 2.4.** $f_1 - f_4$ functions

| | |
|---|---|
| $f_1(G)$ | Glucose dependent production of plasma insulin |
| $f_2(G)$ | Insulin independent glucose utilization (brain) |
| $f_3(I_i)$ | Insulin dependent glucose utilization (remote tissues) |
| $f_4(h_3)$ | Insulin dependent glucose production |

$$f_1(G) = \frac{R_m}{1 + exp(\frac{-G}{V_g C_1} + a_1)} \tag{2.7}$$

$$f_2(G) = U_b[1 - exp(\frac{-G}{C_2 V_g})] \tag{2.8}$$

$$f_3(I_i) = \frac{1}{C_3 V_g}(U_0 + \frac{U_m - U_0}{1 + (kI_i)^{-}\beta}) \tag{2.9}$$

$$k = \frac{1}{C_4}(\frac{1}{V_i} + \frac{1}{Et_i}) \tag{2.10}$$

$$f_4(h_3) = \frac{R_g}{1 + exp[(\alpha(\frac{h_3}{C_5 V_p} - 1))]} \tag{2.11}$$

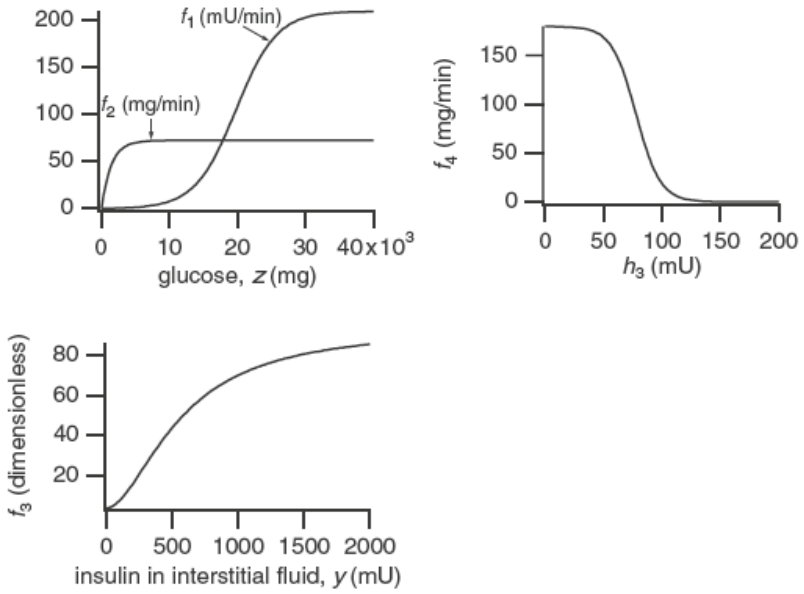


**Figure 2.3.** Functions $f_1 - f_4$ [3]

Sturis et al. note that the amplitude of ultradian oscillations depends critically upon the shape of $f_1$ and $f_4$. For instance, if the slope of either of these curves is decreased by 10-20%, the oscillations become steeply damped.

In their original paper, Sturis et al. write many of the parameters inside of $f_1 - f_4$ as constants with given values. These parameters do not have any physical meaning, and are designed to optimize the ultradian oscillatory behavior by shaping the function in such a way that the oscillation amplitude is maximized.

Sensitivity Analysis

The parameters $t_1, t_2, t_3, E, V_1, V_2$, and $V_3$ have values with physical meaning which are derived from literature. Sturis et al. performed a partial sensitivity analysis, holding all parameters constant except for one and monitoring the range of values which demonstrate ultradian oscillatory behavior.

**Table 2.5.** Sensitivity Analysis

| **Parameters** | **Base Value** | **Range with Oscillations** |
|---|---|---|
| $T_1$(seconds) | 6 | 4-8 |
| $T_2$(seconds) | 100 | 60-140 |
| $T_3$(seconds) | 36 | 25-50 |
| E(liters/min) | 0.2 | 0.1-0.3 |
| $V_1$(liters) | 3 | 2-4 |
| $V_2$(liters) | 11 | 7-15 |
| $V_3$(liters) | 10 | 7-13 |

## 2.4 Longevity of the Sturis Model, and New Models

The model from Sturis et al has been used often since its inception in 1991, and remains a strong choice for analyzing glucose and insulin dynamics. However, the model is a high-level representation of a very complex system with many subtle interacting components. The model proposed in Han et al [6] extends the Sturis

model to encapsulate $\beta$-cell insulin releasing behavior. This amounts to a redesign of the function $f_1$ from Sturis et al, which represents the release of plasma insulin in response to the presence of glucose. In time, contributions like this may lead to an extended Sturis model in which all parameters can be mapped to cellular physiology. The model in Han et al. produces glucose/insulin behavior with short, long, and ultradian oscillations similar in form to those from the Sturis model.

# Chapter 3
# Data Assimilation Method

## 3.1 Unscented Kalman Filter

### 3.1.1 Introduction

Data assimilation is a prediction correction scheme for estimating the state of a system through the use of a mathematical model to predict future states, and statistical inference to correct the projected state using measured values of one or more model variables. Both the model and measurements are assumed to have stochastic components, such that a probability distribution of the state is propagated and corrected over time.

In this work, the Sturis model is employed to propagate model state, and measurements of glucose are used to correct the state probability distribution. In Chapters 5 and 6, data assimilation is employed to infer (and thus reconstruct) the rate of feeding for healthy and comatose patients.

The Unscented Kalman Filter is a data assimilation scheme particularly well-suited to the nonlinear problem of glucose/insulin dynamics due to its correction for linearization error. Chapter 3 includes a description of the Unscented Kalman Filter, and a discussion of its potential for use in reconstructing the behavior of unmeasured glucose/insulin variables.

### 3.1.2 Overview of Kalman Filter

The Unscented Kalman Filter is a type of sigma-point Kalman filter for linearizing a nonlinear function. The defining characteristic of the Unscented Kalman Filter is the development of a sigma point estimator for model state distribution. Sigma points are selected to represent the state distribution, and are then integrated forward through time. This is a different approach than the Extended Kalman Filter, which relies on analytic solution to perpetuate the state distribution. Once the sigma points are integrated forward through a nonlinear process model, the mean and covariance are reconstructed.

### 3.1.3 Unscented Transform

Unscented transformation is the procedure of selecting sigma points based upon an initial mean and covariance, integrating through a process model, and computing a final mean and covariance.

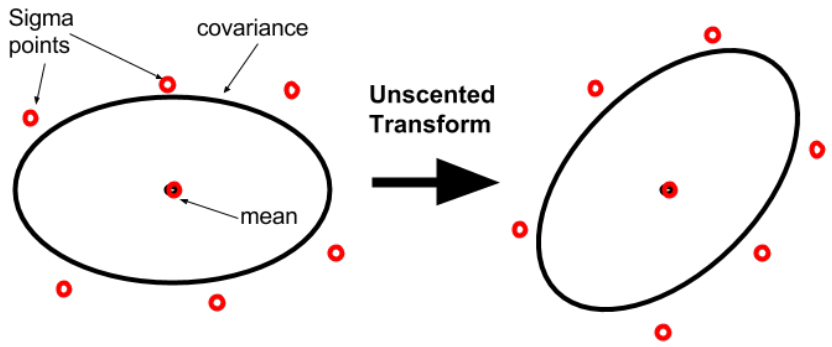


**Figure 3.1.** The Unscented Transformation

The model requires knowledge of an initial state $x_0$, with mean $\mu_0 = E[x_0]$ and covariance $P_0 = E[(x_0 - \mu_0)(x_0 - \mu_0)^T]$.

Selection of Sigma Points The state distribution is characterized by $2n+1$ sigma points, where $n$ is the dimension of the state space. Included below is the set of equations for calculating sigma points, from [7].

$$X_k - 1 = (x_k^i - 1, W^j) | j = 0...2n \tag{3.1}$$

$$X_k^0 - 1 = X_k^a - 1 \tag{3.2}$$

$$-1 < W^0 < 1 \tag{3.3}$$

$$X_k^i - 1 = X_k^a - 1 + (\sqrt{\frac{n}{1 - W^0} P_k - 1}), i = 1...n \tag{3.4}$$

$$X^i + n_k - 1 = X_k^a - 1 - (\sqrt{\frac{n}{1 - W^0} P_k - 1}), i = 1...n \tag{3.5}$$

$$W^i = \frac{1 - W^0}{2n}, j = 1...2n \tag{3.6}$$

Points where $W^0 >= 0$ are further from the origin, while points where $W^0 <= 0$ are closer to the origin.

### 3.1.4 Data Assimilation Step

The Unscented Kalman Filter includes a data assimilation step, where information is introduced from measured values. The set of equations describing this step are reproduced here from [7].

$$X_k^a = X_k^f + K_k(z_k - z_k^f - 1) \tag{3.7}$$

Where $z_k$ is the measured observation, and $z_k^f - 1$ is the value observed from propagation of the nonlinear process model.

$$K_k = Cov(\tilde{x}_k^f, \tilde{z}_k^f - 1)Cov^{-1}(\tilde{z}_k^f - 1) \tag{3.8}$$

$$P_k = P_k^f - K_k Cov(\tilde{z}_k^f - 1)K_k^T \tag{3.9}$$

### 3.1.5 Summary

Linearization of a nonlinear model, such as the Sturis model, introduces error. The Unscented Kalman Filter is well-suited to this class of model, as it represents the uncertainty attributed to linearization errors. Glucose measurements are not continuous, and the dynamical processes underlying glucose/insulin dynamics operate on both short and long time scales. The Unscented Kalman Filter provides a mechanism to track and estimate changes in blood glucose levels between observation times.

## 3.2 Applications in the Intensive Care Unit

While plasma glucose and plasma insulin are both measurable, glucose dynamics also depends on unmeasurable variables. Knowledge of all model variables is useful when making treatment decisions, such as evaluating the need for insulin delivery therapies. Data assimilation techniques are useful as a method of estimating the system state given an incomplete set of measured variables. In [4], Sedigh-Sarvestani et al. demonstrate use of the Unscented Kalman Filter with the Sturis model of glucose/insulin dynamics. They show that it is possible to reconstruct the system state to an acceptable degree of accuracy using only sparse measurements of one or two variables. Furthermore, they develop an approach to evaluate the similarity between reconstructed and true system dynamics, and use it to determine which variables should be measured to optimize reconstruction accuracy.

To derive a quantitative representation of reconstruction accuracy, Sedigh-

Sarvestani et al. introduce the Empirical Observability Coefficient (EOC):

$$EOC = \frac{1}{1+\epsilon_i^2} \tag{3.10}$$

where $\epsilon_i^2$ is defined as the mean squared difference between true and reconstructed dynamics, normalized by the variance of the true dynamics.

$$\epsilon_i^2 = \frac{< (x_i - \widetilde{x}_i)^2 >}{var(x_i)} \tag{3.11}$$

By varying which one of the model variables is measured, Sedigh-Sarvestani et al. use the EOC to identify the optimal variables to measure for accurate state reconstruction.

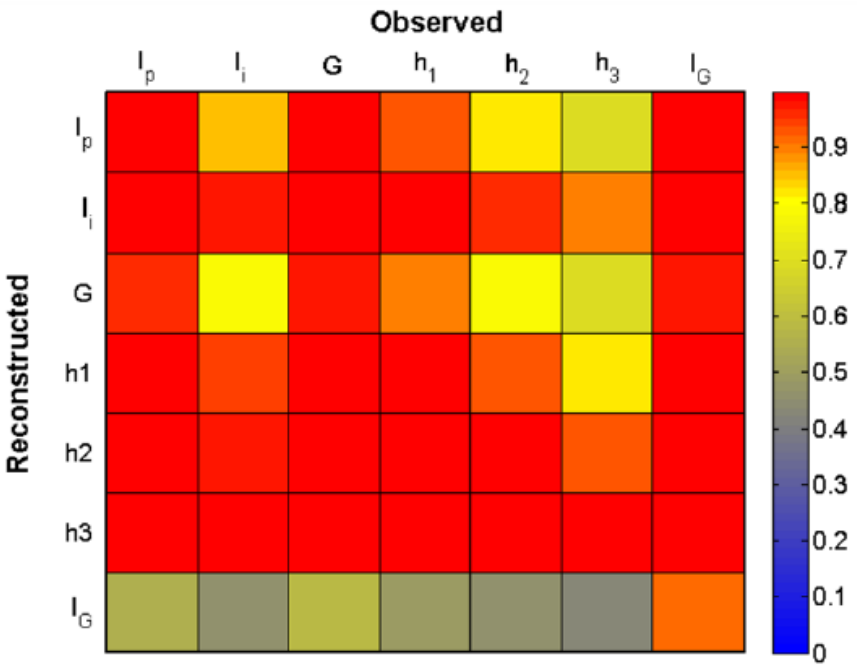


**Figure 3.2.** EOC values when one variables is measured [4]

Plasma glucose, plasma insulin, and the feeding function ($I_G$) are the best variables to measure for successfully reconstructing all other variables.

The data introduced in chapters 5 and 6 consists of measurements of glucose and feeding. Figure 4 provides an important validation that it is reasonable to attempt state estimation using measurements of these two variables. In addition, it suggests that some benefit might be derived from measurements of plasma insulin. While techniques do exist to measure plasma insulin [8], widely available commercial products do not yet exist. This work does not include data with plasma insulin measurements.

## 3.3 Unscented Kalman Filter for Glucose and Insulin State Estimation

Benchmarking the Unscented Kalman Filter against other Kalman Filters on glucose dynamics tasks shows that the former produces more accurate reconstructions. In an effort to quantize the performance differences of Extended, Unscented, and Ensemble Kalman Filters, Miller [5] computes the root-mean-square error of reconstructed glucose dynamics for each method on 180 minutes of data produced using the Bergman minimal model. The equations of the Bergman model are elaborated in [9]. Like the Sturis model, the Bergman minimal model has three pools: plasma glucose, plasma insulin, and interstitial insulin. Also similar is the nonlinear behavior this model exhibits. The Unscented Kalman Filter performs well on systems that are highly nonlinear, which makes it a good choice for studying the Bergman and Sturis models of glucose dynamics. The root-mean-square error (RMSE) is calculated according to the formula:

$$RMSE = \sqrt{\frac{1}{k}\sum_{i=0}^{k}(x_i - \widetilde{x}_i)^2} \tag{3.12}$$

where $k$ is the total number of points at which measurements are simulated. An interesting result from [5] is the superiority of the Unscented Kalman Filter for

state estimation when compared to the Extended Kalman Filter and the Ensemble Kalman Filter.

**Table 3.1.** Kalman Filter Comparison [5]

| | **Extended Kalman Filter** | **Unscented Kalman Filter** | **Ensemble Kalman Filter** |
|---|---|---|---|
| Compute Time (s) | 0.02 | 6.02 | 121.61 |
| RMSE Plasma Glucose (mg/dL) | 1.05 | 0.55 | 1.84 |
| RMSE Plasma Insulin ($\mu$U/mL) | 12.24 | 0.39 | 0.47 |

The above RMSE values are for Kalman filters with values initialized fairly accurately. Poor initialization will result in a much RMSE for all filters, although the error will diminish over time as the filters converge. It is worthy to note that the computation time required by the Unscented Kalman Filter is somewhat greater than the Extended Kalman Filter, and substantially less than the Ensemble Kalman Filter. The Unscented Kalman Filter demonstrates accurate performance on nonlinear systems, and is well-suited to studying glucose/insulin dynamics.

## 3.4 Sturis Model Applied to Electronic Health Record Data

Collecting blood glucose and feeding data over long time scales involves overcoming challenges such as high expense, inconsistency of measurement techniques, and irregularity of measurement time intervals. An alternative introduced in [10] by Albers et al. is to repurpose data collected for another reason. The Intensive Care Unit (ICU) records blood glucose and feeding, motivated by their patients' inability to consume food unassisted. The Electronic Health Record thus contains a volume

of glucose and feeding data of high enough quality to be of practical interest for studying glucose dynamics.

In [10], Albers et al. raise some of the unique challenges and benefits associated with using Electronic Health Record data to study physiological phenomena. Some of the notable drawbacks include abnormalities due to patient disease or trauma (and the lack of a control group to help identify such bias), and inconsistent measurement techniques. Furthermore, when evaluating Electronic Health Record data against a mathematical model, it is important to account for the high degree of individual variability amongst patients. An advantage of using Electronic Health Record data is the existence of data with atypical feeding functions compared to the habitual eating cycles of humans. One example is the approximately continuous feeding function which results from a steady glucose drip. Continuous feeding data is useful in characterizing the undamped oscillatory behavior of glucose and insulin.

## 3.5 Bolus Estimation with UKF

Accurate estimation of carbohydrate consumption is challenging when nutrition information is not available, or when portion size is not a multiple of the serving size. For patients with type I Diabetes, flawed estimation of carbohydrate content in their food might result in mismanagement of insulin therapy. Patients who utilize an insulin pump may benefit from withholding insulin treatment until 15-30 minutes after consuming a meal [11]. This delay enables computational estimation of the size of the glucose bolus. Then, the blood glucose can be optimized by using a prediction of future glucose dynamics to determine how much insulin to release.

The detailed algorithm for insulin dosage optimization with the Unscented Kalman Filter can be found in [11]. A non-linear model of glucose dynamics is used to predict future glucose behavior, and insulin delivery is iteratively optimized such that the average glucose is as close to some "target glucose" value for the

maximum amount of time possible. The work in [11] demonstrates the Unscented Kalman Filter as a successful technique for glucose bolus size estimation.

## 3.6 Frequency Characterization

Glucose dynamics involves periodic elements on widely varying time scales, ranging from minutes to hours to days. Gough et al. show that 10 minutes is the minimum measurement frequency necessary to characterize the glucose dynamics of normal subjects and some diabetic subjects [12]. The maximum acceptable sampling interval is called the Nyquist Sampling Period. The Nyquist Sampling Frequency (the inverse of the Nyquist Sampling Period) is computed according to the following formula:

$$W_{NSR} >= 2W_{BE}$$

where $W_{NSR}$ is the Nyquist Sampling Frequency, and $W_{BE}$ is the band edge frequency.

Knowledge of the Nyquist Sampling Frequency is important when constructing a state estimate of the glucose/insulin system based on sparse data. The Sturis model is designed to simulate ultradian oscillations in glucose and insulin. A maximum measurement interval of 10 minutes will provide enough data points on each ultradian period to align the phase of reconstructed oscillations with that of the true oscillations. Gough et al. suggest using a 10-minute maximum measurement interval as a guideline when designing implantable continuous plasma glucose monitoring systems. It will also serve as a standard for evaluating whether an existing dataset has sufficiently frequent measurements to be a strong candidate for reconstruction with the Unscented Kalman Filter.

In [12], Gough et al. acknowledge the scarcity of continuous measurements of glucose which meet their criteria of a 10-minute maximum measurement interval.

In particular, little such data exists for non-diabetic subjects. This represents a limitation to their result, since the complexity of glucose/insulin dynamics is reduced in diabetic patients [13]. Therefore, the Nyquist Sampling Period may be less than 10 minutes in some non-diabetic people. Such data is not likely to become widely available until continuous glucose monitoring techniques become less costly and less invasive.

### 3.6.1 Summary of Data Assimilation

In Chapter 3, we have seen that sporadic measurement of some variables of the glucose/insulin system presents a data assimilation problem. The Unscented Kalman Filter is a good choice of data assimilation scheme for nonlinear systems, and has been successfully applied to the reconstruction of unmeasured variables in simulation with the Sturis model [4]. This technique will be applied in Chapters 5 and 6 to reconstruct the feeding function by statistical inference using measurements of glucose in healthy (Chapter 5) and comatose (Chapter 6) patients.

# Chapter 4
# Model Characterization

## 4.1 Integrating the Sturis Model

During data assimilation of glucose/insulin dynamics in this paper, the Sturis model is employed to propagate model dynamics between measurements. The model includes 20 parameters and 7 variables, where the feeding function has been treated as a variable. Most parameters affect the shape of $f_1 - f_4$, and model dynamics may change dramatically upon subtle changes to these values. The case of continuous, steady-state feeding is a suitable starting point for studying the Sturis model for several reasons.

1. Using parameter values given in [2], the model will demonstrate undamped periodic oscillatory behavior in all variables.

2. A primary aim of [2] was to devise a glucose/insulin model which included ultradian oscillations. Therefore, the parameters given in that paper will produce high-amplitude ultradian oscillations compared to other parameter selection possibilities.

**Table 4.1.** Default Parameter Values

| **Parameter** | **Default Value** | **Significance** |
|---|---|---|
| $V_p$ | 3 L | Plasma insulin volume |
| $V_i$ | 11 L | Interstitial insulin volume |
| $V_g$ | 10 L | Plasma glucose volume |
| $E$ | 10 L | Exchange rate for interstitial insulin and plasma insulin |
| $t_p$ | 6 min | Time constant for plasma insulin degradation |
| $t_i$ | 100 min | Time constant for interstitial insulin degradation |
| $t_d$ | 12 min | Time constant for linear filter |
| $R_m$ | 209 mU/min | Scaling constant for glucose dependent plasma insulin generation |
| $a_1$ | 6.67 | Affects the shape of $f_1$ |
| $C_1$ | 300 mg/L | Scales inversely with $f_1$ |
| $C_2$ | 144 mg/L | Scales directly with $f_2$ |
| $C_3$ | 100 mg/L | Scales inversely with $f_3$ |
| $C_4$ | 80 mU/L | Scales inversely with $f_3$ |
| $C_5$ | 26 mU/L | Scales directly with $f_4$ |
| $U_b$ | 72 mg/min | Scaling constant for insulin independent glucose utilization |
| $U_0$ | 4 mg/min | Affects the shape of $f_3$ |
| $U_m$ | 94 mg/min | Affects the shape of $f_3$ |
| $R_g$ | 180 mg/min | Scaling constant for insulin dependent glucose production |
| $\alpha$ | 7.5 | Scales inversely with $f_4$ |
| $\beta$ | 1.77 | Scales directly with $f_3$ |

**Table 4.2.** Initial Values of Variables

| **Variable Name** | **Initial Value** |
|---|---|
| $I_p$ - Plasma Insulin | 200 mIU/L |
| $I_i$ - Interstitial Insulin | 200 mIU/L |
| $G$ - Plasma Glucose | 12000 mg/DL |
| $h_1$ - Linear Filter Step 1 | 0.1 mIU/L |
| $h_2$ - Linear Filter Step 2 | 0.2 mIU/L |
| $h_3$ - Linear Filter Step 3 | 0.1 mIU/L |

The feeding function for this simulation is constant, at 216 mg/min. Non-constant feeding functions are simulated in section 4.2.

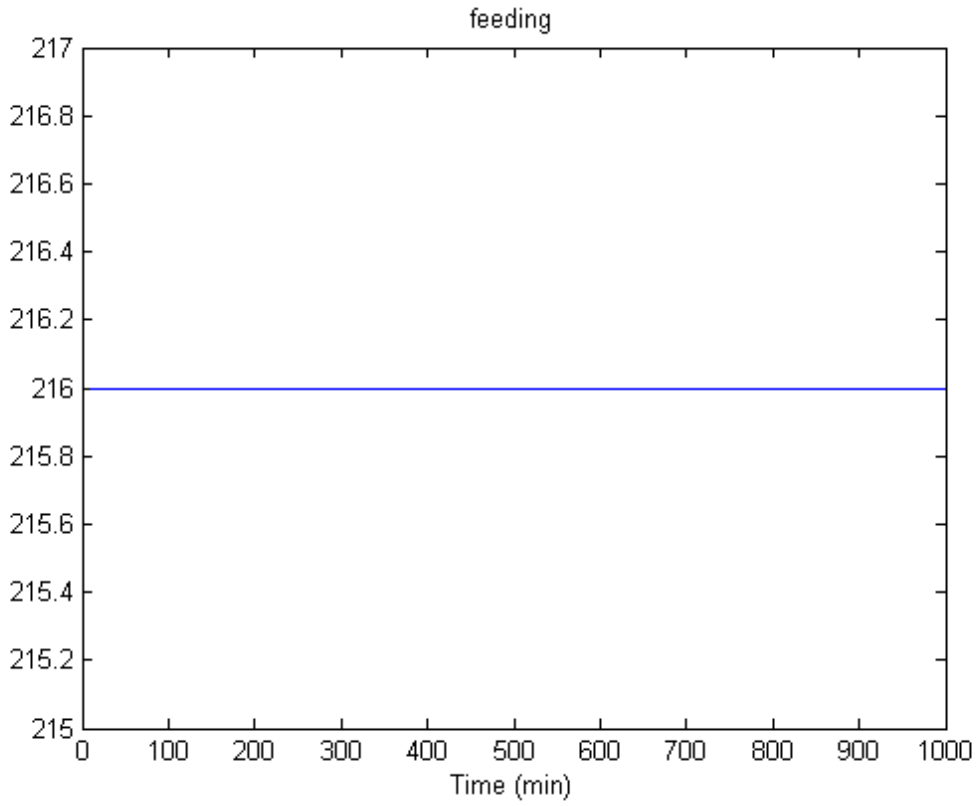


**Figure 4.1.** Steady-State Feeding Function vs. Time

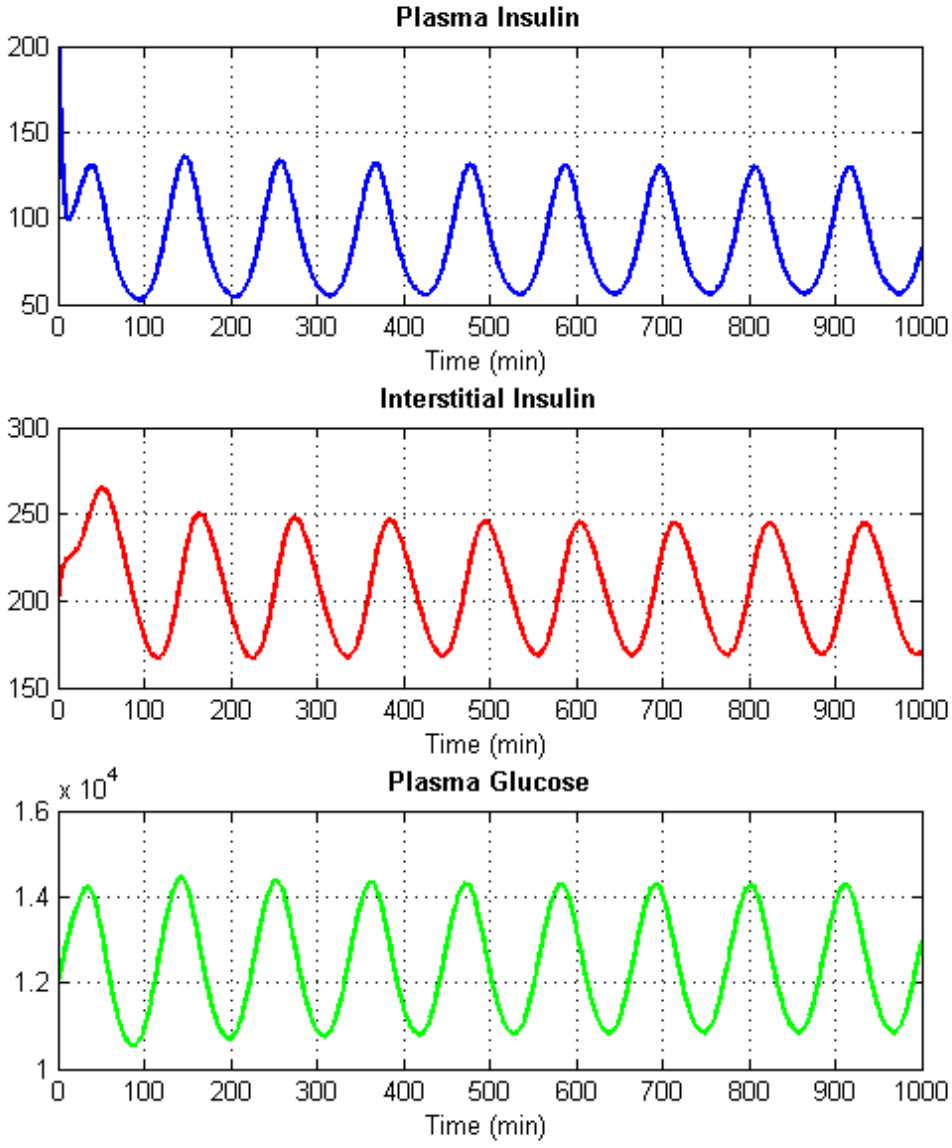


**Figure 4.2.** Glucose and Insulin with Steady-State Feeding

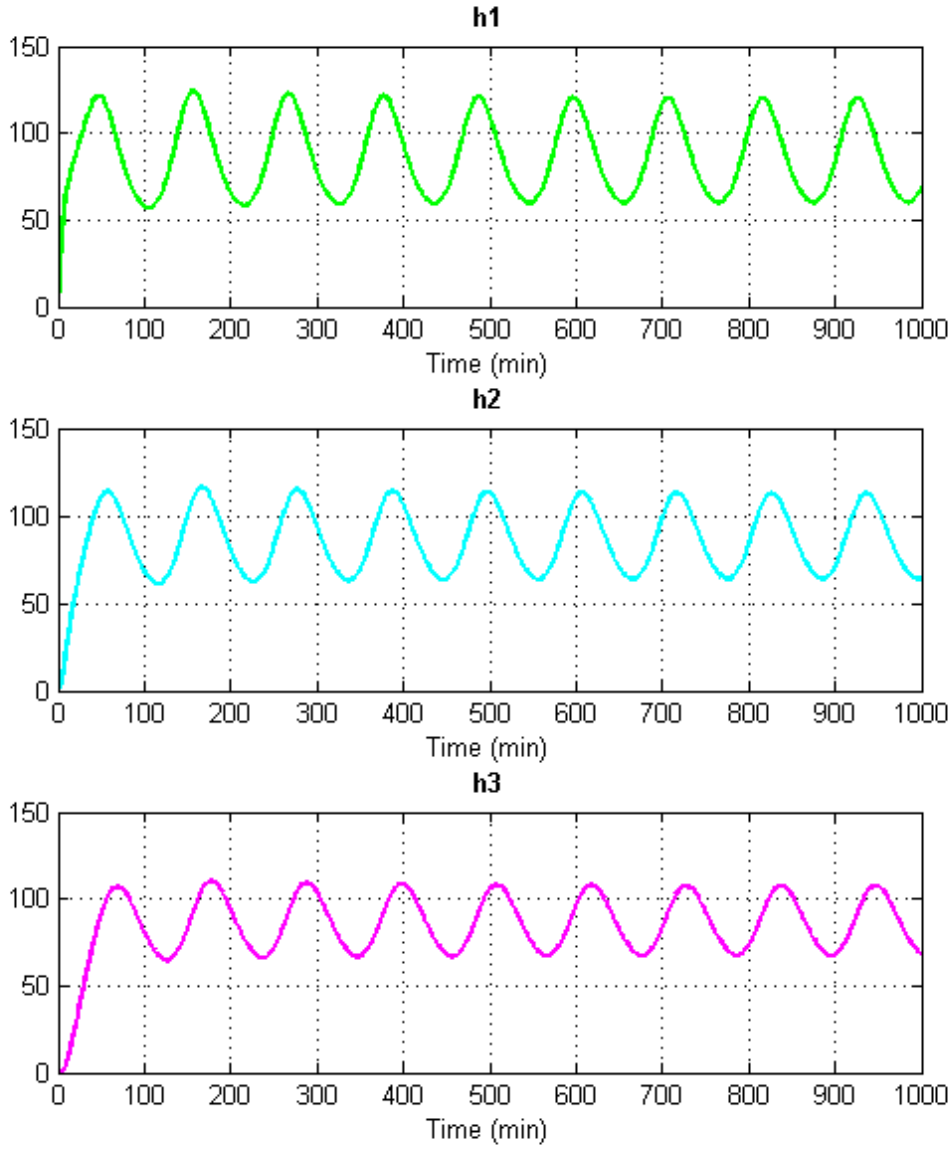


**Figure 4.3.** Linear Filter $h_1$-$h_3$ with Steady-State Feeding

The simulation presented in figures above has a time step of one minute, and was run for 1000 time steps. Because the default parameter values are used and the feeding function is both constant and sufficiently large, all model variables demonstrate ultradian oscillatory behavior. For all variables, oscillations maintain

**Table 4.3.** Mean Variable Values

| **Variable** | **Mean Value** |
|---|---|
| $I_p$ - Plasma Insulin | 87.2 mIU/L |
| $I_i$ - Interstitial Insulin | 207.2 mIU/L |
| $G$ - Plasma Glucose | 12414 mg/DL |
| $h_1$ - Linear Filter Step 1 | 86.3 mIU/L |
| $h_2$ - Linear Filter Step 2 | 85.5 mIU/L |
| $h_3$ - Linear Filter Step 3 | 84.7 mIU/L |

nearly constant amplitude after 100 - 200 minutes. Due to imperfect initial conditions, the first one or two oscillation periods may have a larger or smaller amplitude than subsequent oscillations. This effect is particularly noticeable in the linear filter, since $h_1$, $h_2$, and $h_3$, are initialized with values much smaller than they will tend to hold after the first few time steps. Note that plasma insulin is initialized at 200 mIU/L, while the mean plasma insulin value is 87.2 mIU/L.

The Sturis model is designed such that changes in plasma insulin follow changes in plasma glucose, after a short time delay. This fact is verified in the figure below by overlaying glucose and insulin values from minutes 200-400 in the above simulation. Both glucose and insulin values have been normalized by their average oscillation amplitudes (3910 and 83, respectively).

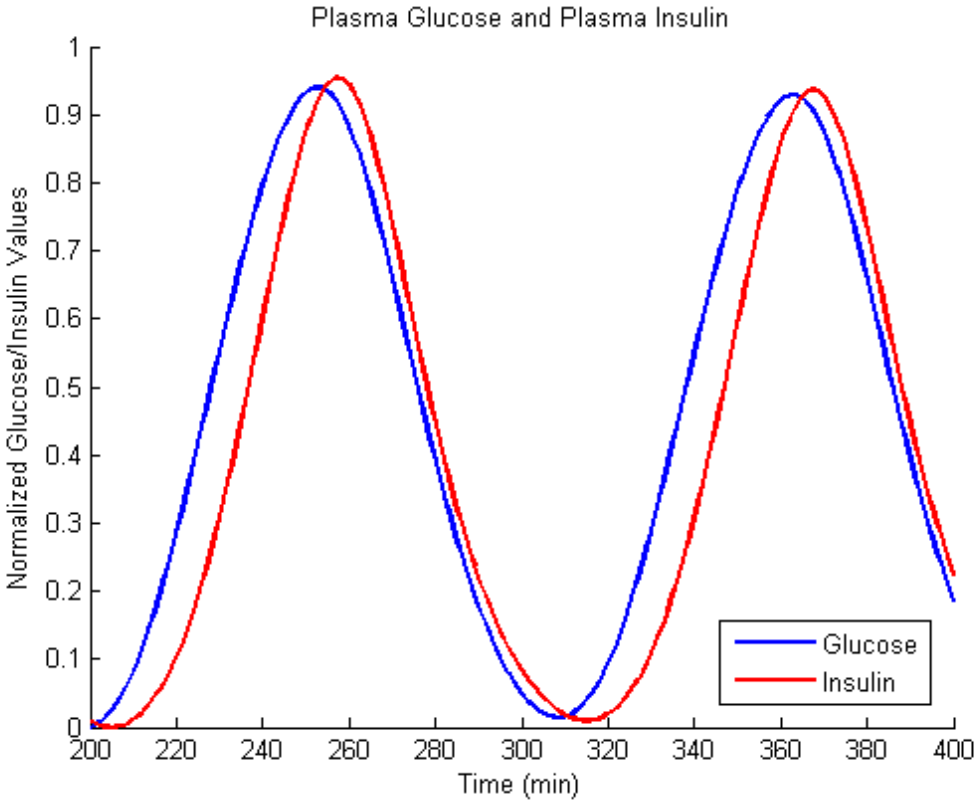


**Figure 4.4.** Normalized Plasma Glucose and Plasma Insulin Oscillations

Changes in plasma glucose lead changes in plasma insulin by a time delay of no more than ten minutes. This behavior is a trait of the Sturis model, and was motivated by experimental measurements which showed that plasma insulin is directly related to plasma glucose concentrations after a time delay of 10-20 minutes [2].

## 4.2 Glucose Behavior with Various Feeding Functions

### 4.2.1 Step Changes in the Feeding Function

In the Neuro-ICU, patients receive feeding at a steady rate. As the person's blood glucose level changes, caretakers may adjust the rate of feeding. Such a

change will present as an abrupt step in the patient's feeding. In the Sturis model, glucose/insulin oscillations may change in amplitude and mean value when a step change in feeding occurs. To demonstrate this behavior, glucose and insulin behavior during a step change of +50 mg/min and -50 mg/min is plotted below.

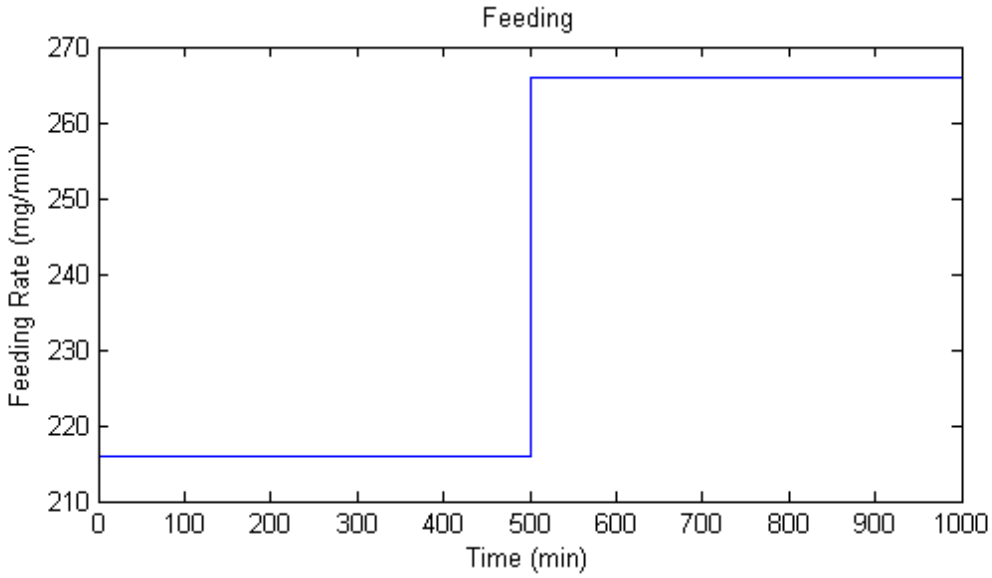


**Figure 4.5.** Step increase in feeding of 50 mg/min

At $t = 500min$, the feeding rate is increased from 216mg/min to 266mg/min.

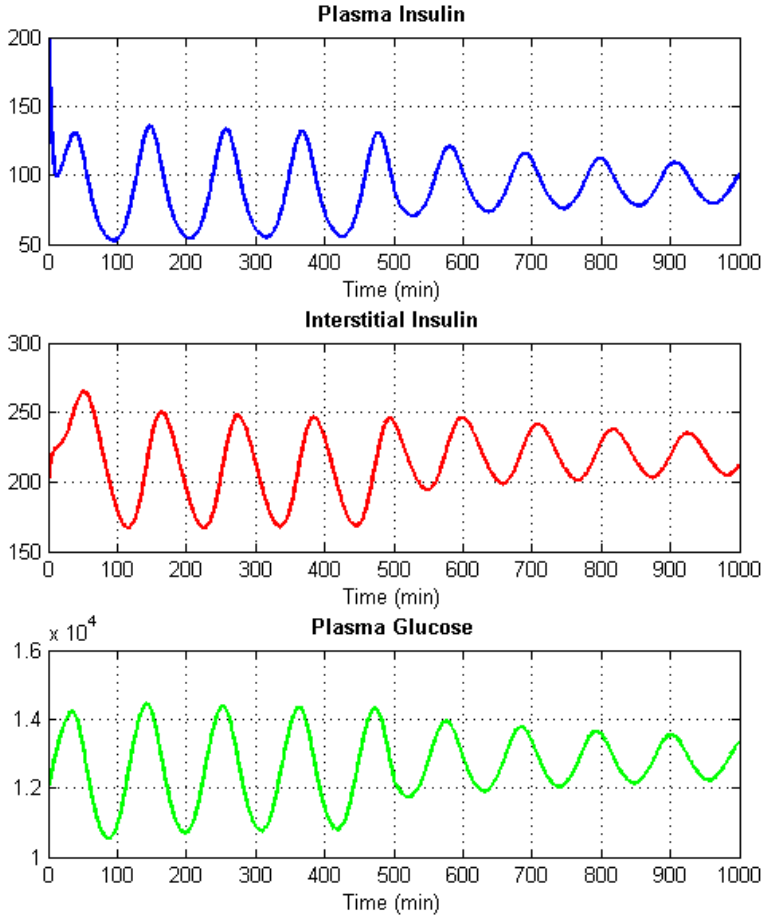


**Figure 4.6.** Glucose and Insulin Behavior upon 50 mg/min step increase in feeding

Prior to the step change in feeding, the mean plasma glucose value is 125mg/dL. After the step change, when the feeding is 266mg/min, the mean plasma glucose value is 128mg/dL. The oscillation amplitude of plasma glucose decreases from 31.02mg/dL to 17.48mg/dL at the step change in feeding.

At $t = 500min$, the feeding rate is decreased from 216mg/min to 166mg/min.

Prior to the step change in feeding, the mean plasma glucose value is 125mg/dL. After the step change, when the feeding is 166mg/min, the mean plasma glucose value is 119mg/dL. The oscillation amplitude of plasma glucose increases from 31.02mg/dL to 41.20mg/dL at the step change in feeding.

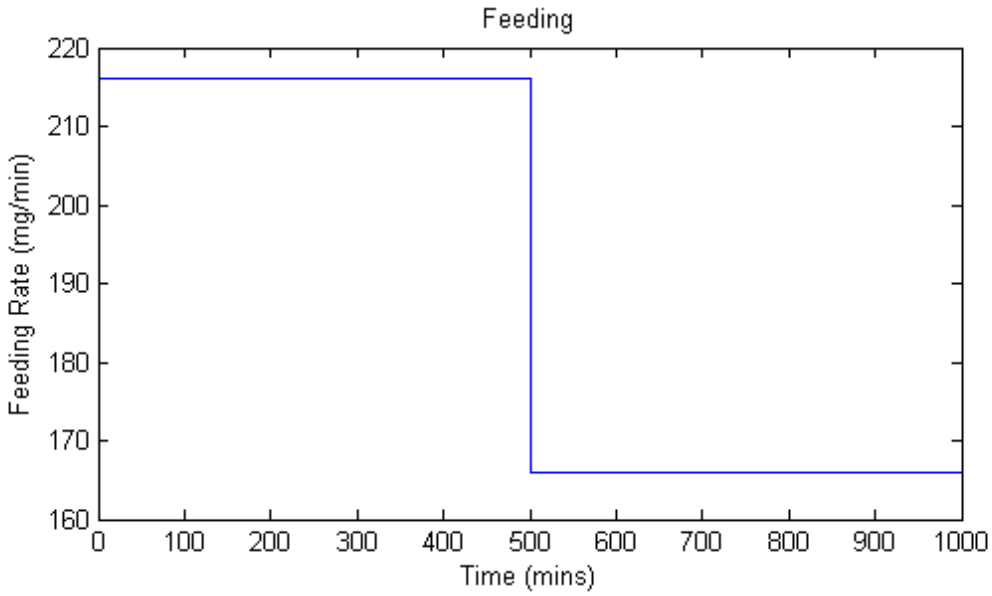


**Figure 4.7.** Step decrease in feeding of 50 mg/min

Increasing the rate of feeding leads to an increase in the mean glucose and insulin levels, while decreasing the rate of feeding results in decreased mean glucose and insulin levels. It is interesting that the amplitude of ultradian oscillations increases when the rate of feeding is decreased from 216mg/min to 166mg/min. A high glucose oscillation amplitude raises the risk involved in making treatment decisions based upon sparse glucose measurements. Without continuous monitoring of plasma glucose, it may be challenging to identify a patient's mean plasma glucose level. Therefore, the decision may be made to lower the rate of feeding for a patient whose glucose is measured near the maximum value in its ultradian cycle even though the mean glucose value is already optimal.

### 4.2.2 Cessation of Oscillations at High Feeding

When the feeding rate is very high, glucose and insulin will saturate and fail to oscillate. The value of saturation is proportional to the feeding rate. Extremely high feeding rate can result in a very high and stable plasma glucose value that would lead to hyperglycemia in a patient.

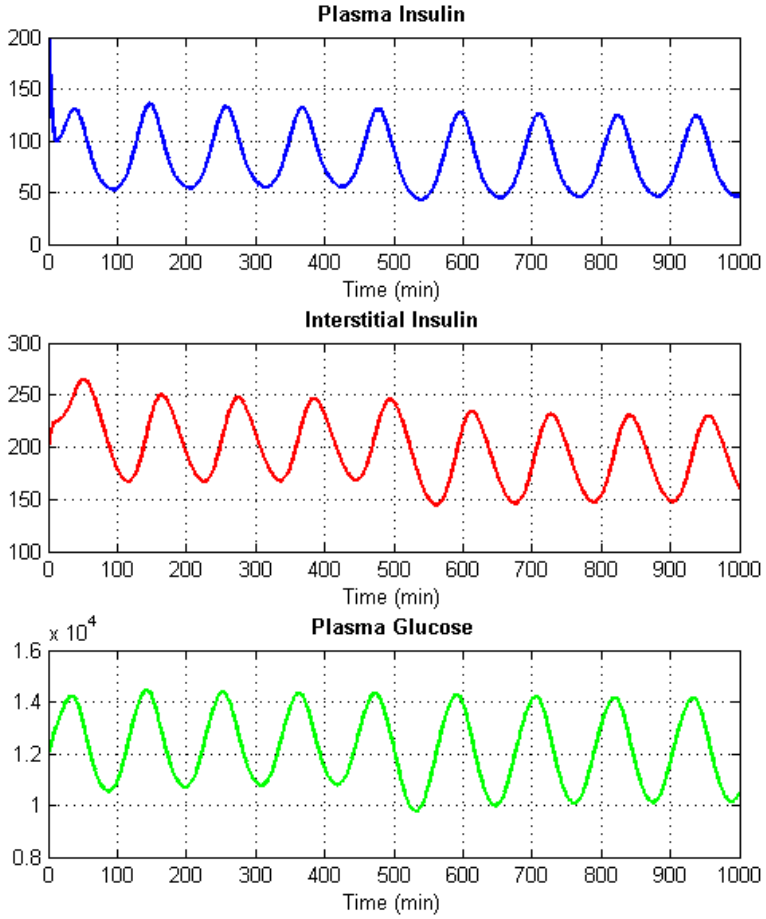


**Figure 4.8.** Glucose and Insulin Behavior upon 50 mg/min step decrease in feeding

After the feeding rate is increased to 466mg/min, glucose and insulin experience a damped ultradian oscillations for several periods before arriving at a stable equilibrium. After 700min, the mean plasma glucose and plasma insulin values are 141.19mg/dL and 135.2mIU/L, respectively.

### 4.2.3 No Feeding

Due to the feedback loop between plasma insulin and plasma glucose production, feeding is not necessary to maintain nonzero glucose and insulin levels in the Sturis

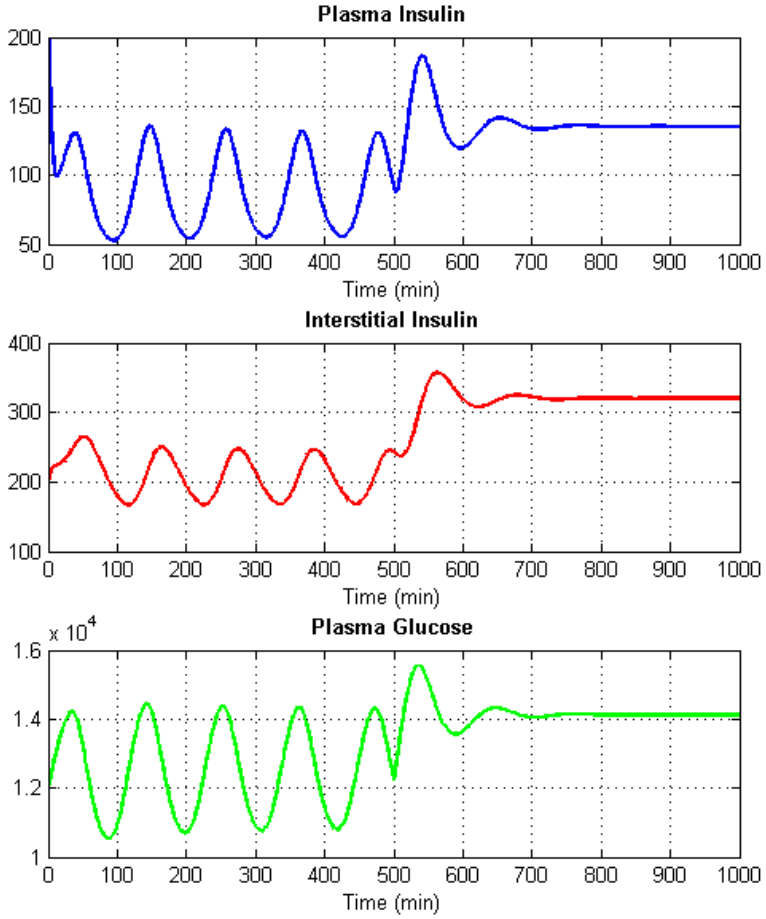


**Figure 4.9.** Step increase in feeding from 216mg/min to 466 mg/min

model. When the rate of feeding is zero, glucose and insulin will move towards a stable equilibrium.

In the figure above, the rate of feeding is 216mg/min from 0-500 min, changing instantaneously to 0mg/min at 500 min. Upon cessation of feeding, glucose and insulin values initially decrease rapidly. However, between 600-800min, the behavior demonstrates damped oscillations with a decreasing amplitude over time. The mean plasma glucose and plasma insulin values after 700min are 108mg/dL and 48.9mIU/L, respectively.

Fasting blood glucose in non-diabetics is considered normal when less than

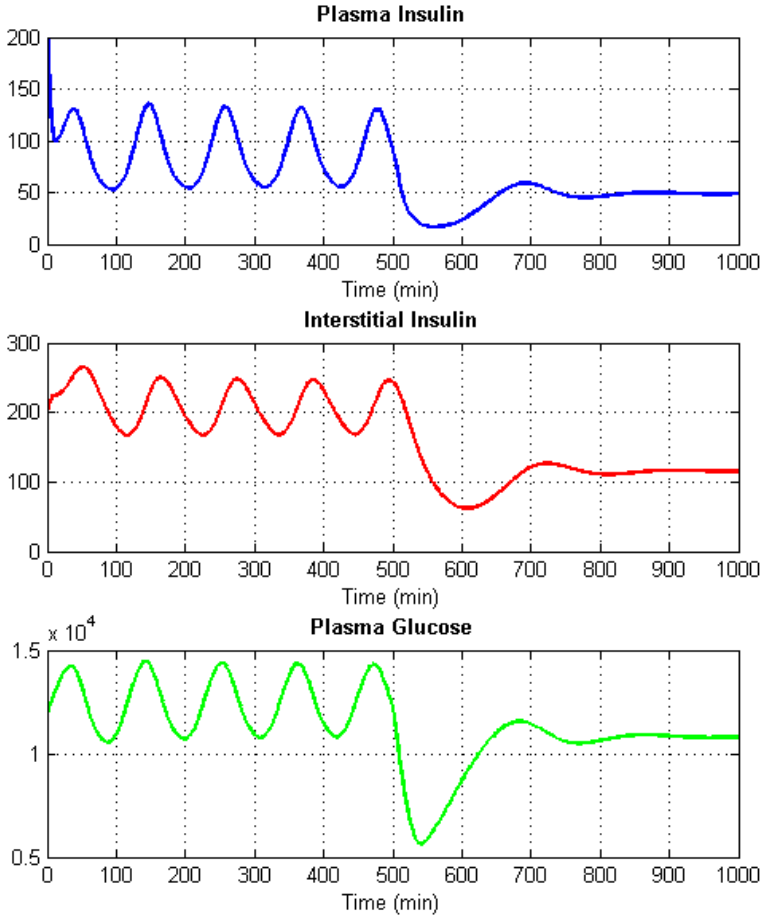


**Figure 4.10.** Step decrease in feeding from 216mg/min to 0 mg/min

100mg/dL. Diabetic patients typically have a fasting blood glucose of 100-125mg/dL, while non-diabetics tend to maintain a fasting blood glucose level between 80-100mg/dL [14]. It is interesting that the Sturis model, with default parameter values, yields a fasting blood glucose level which is typical of a diabetic patient (108mg/dL).

### 4.2.4 Meals with Gradual Absorption and Decay

Glucose is absorbed in the body over time during digestion. To represent a meal in the Sturis model, it is necessary to express the total calories of the meal as a rate of feeding over some window of time. The meal should be represented by a rapid increase in feeding rate, followed by a gradual decay in the feeding rate. Details of the feeding curve shape for a meal will depend upon the type of food consumed, as well as the physiology of the individual who has consumed the meal. An example representation of a meal feeding curve is presented in the figure below.

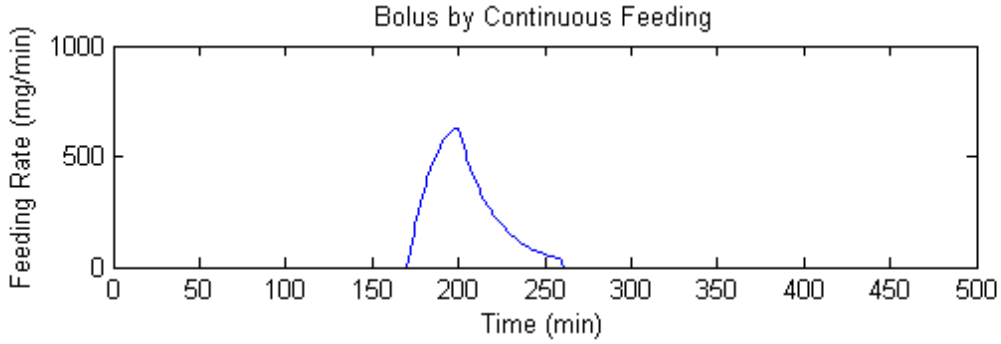


**Figure 4.11.** A continuous rate of feeding curve for a 100 calorie meal

This meal curve has hyperbolic behavior from 170-200 minutes, and decays exponentially from 200-260 minutes.

Hyperbolic Portion:

$$FeedingRate = nCal * \frac{250mgGlucose}{1Cal} * \frac{-(t - t_M)^2 + 900}{36000}, t_M - 30 \leq t < t_M \quad (4.1)$$

Exponential Portion:

$$FeedingRate = nCal * \frac{Exp(\frac{-(t-t_M)}{21})}{40}, t_M \leq t \leq t_M + 60 \quad (4.2)$$

where $n$ is the total number of calories in the meal, and $t_M$ is the time at which the rate of feeding reaches a maximum.

The constants in the above equations are selected such that

$$\int_{t_M-30}^{t_M+60} FeedingRate = nCal \tag{4.3}$$

An example of the glucose and insulin behavior from a meal of this shape is given below.

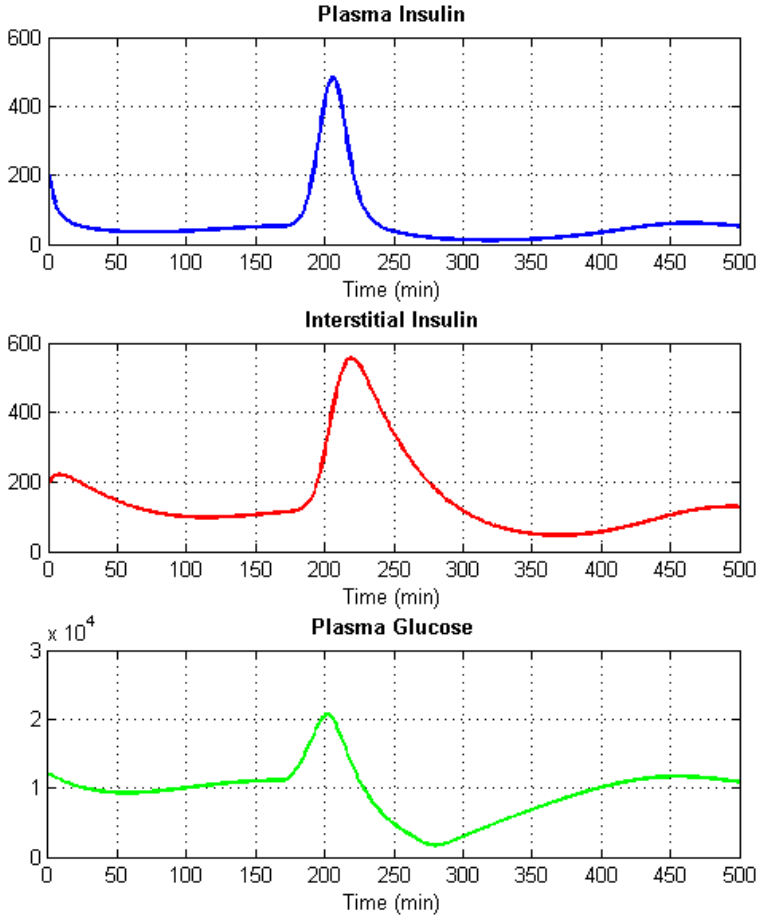


**Figure 4.12.** Glucose and Insulin Behavior for Meal Feeding

The rate of feeding is 0mg/min from 0-170min, follows the meal curve equations from 170-260min, and returns to 0mg/min at 260min. While glucose initially increases substantially, it reaches a very low minimum of 17.1mg/dL.

## 4.3 Parameters

### 4.3.1 Scaling Parameters

The Sturis model includes 20 parameters. Changing parameter values affects the amplitude of the ultradian oscillations of glucose and insulin. In [2], Sturis et al. characterize the range in which glucose/insulin ultradian oscillations persist when varying one parameter at a time. This result was included in Chapter 2. While this analysis provides a starting point for selecting parameter values that will produce ultradian oscillations, it is insufficient for determining in which direction a parameter should be modified to increase or decrease the oscillation amplitude. Furthermore, many parameters such as $R_g, U_b, C_3$, and $R_m$ are given as constants by Sturis et al, and their effect on the amplitude of ultradian oscillations is not explored in [2]. The figures below characterize the ultradian oscillatory amplitude of glucose with respect to $R_g, U_b, C_3$, and $R_m$.

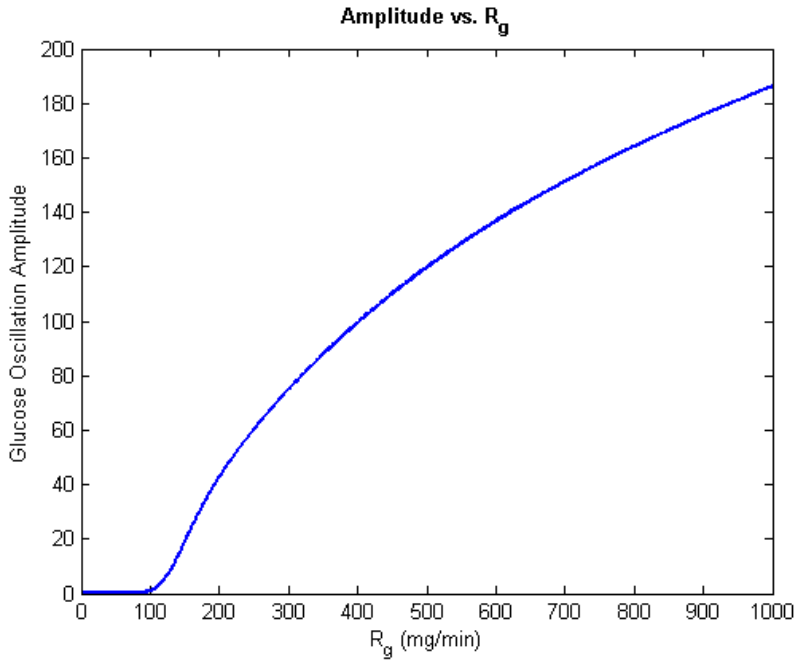


**Figure 4.13.** Scaling factor for plasma insulin dependent glucose production

The default value for $R_g$ is 180mg/min. $R_g$ is the scaling parameter on the function $f_4$, which represents the production of glucose dependent upon the plasma insulin levels after a three-stage linear filter. Increasing the value of $R_g$ increases the proportion of glucose added to the system in response to plasma insulin. Since insulin is produced in response to glucose, the result is a steady increase in the total glucose and insulin in the system. Therefore, as the value of $R_g$ increases, the amplitude of glucose ultradian oscillations will also increase.

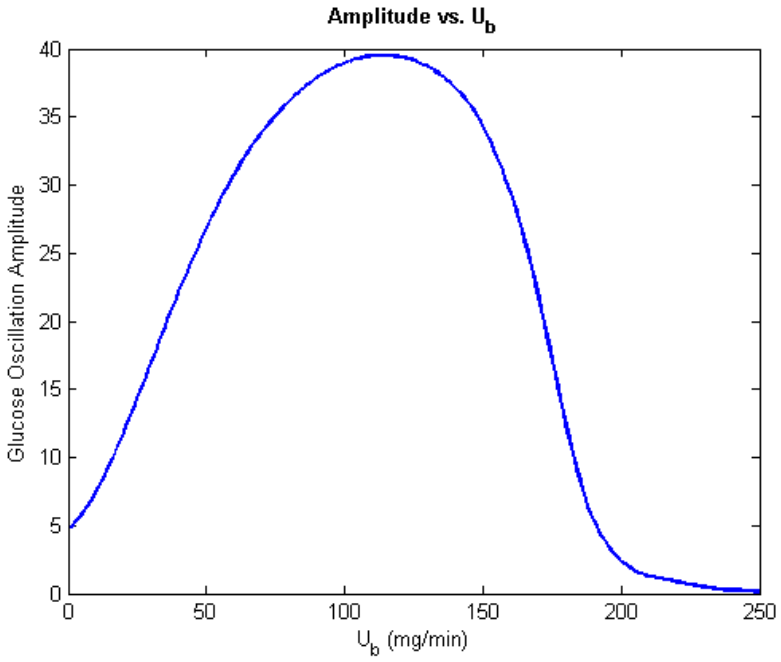


**Figure 4.14.** Scaling factor for insulin independent glucose utilization

The default value for $U_b$ is 72mg/min. At this value, the amplitude of glucose oscillations is 31mg/dL. However, the oscillation amplitude increases to nearly 40mg/dL when $U_b$ is 113mg/min. $U_b$ represents the utilization of glucose that does not rely on interstitial insulin, such as by the brain. If the value of $U_b$ is too small, the glucose oscillations will have reduced amplitude since the minimum glucose value will increase. However, if $U_b$ is too large, the maximum glucose value will decrease. As the maximum glucose value continues to fall, the oscillation amplitude will approach zero when $U_b$ is 250mg/min.

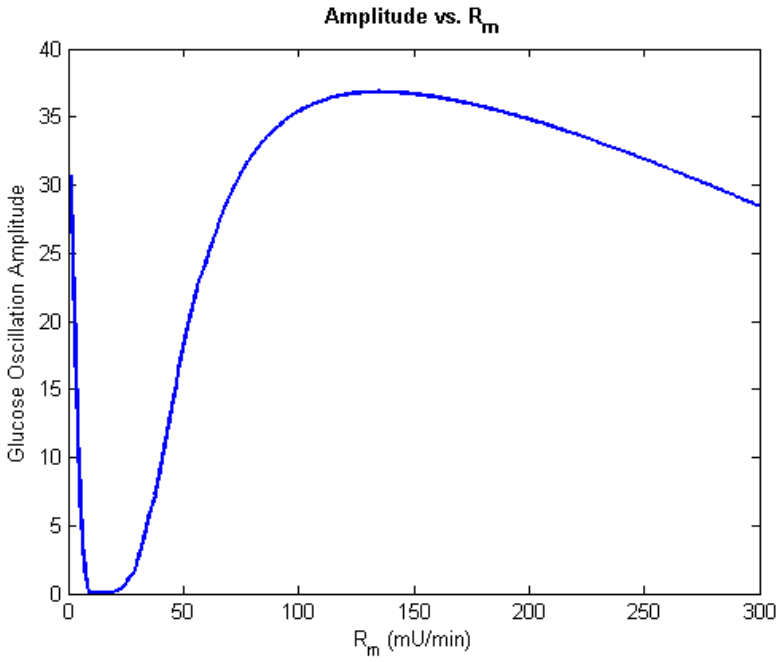


**Figure 4.15.** Scaling factor for glucose dependent plasma insulin production

The default value for $R_m$ is 209mU/min. When $R_m$ is 135mU/min, the oscillation amplitude of glucose is at its maximum value of 36mg/dL. Like $R_g$, $R_m$ must be large enough that insulin is added to the system faster than it decays. However, unlike $R_g$, when $R_m$ is very large, the glucose oscillation amplitude begins to decline even though the amount of glucose added to the system by $f_4$ is directly proportional to the size of $R_m$. This is because plasma insulin must maintain equilibrium with interstitial insulin. Therefore, when $R_m$ is larger than 135mU/min, the glucose oscillation amplitude begins to decline with increasing $R_m$ since more glucose is removed by the term $f_3(I_i)G$ than is added by the term $f_4(h_3)$.

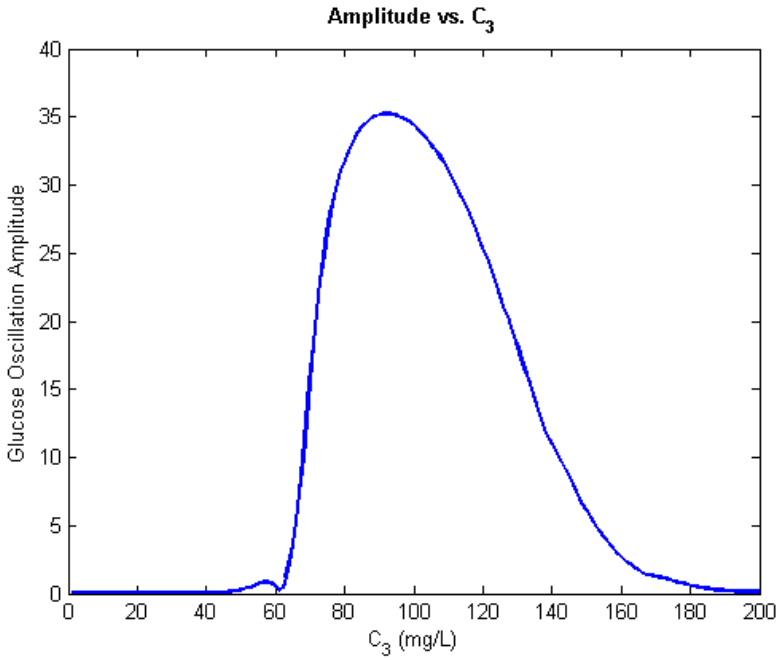


**Figure 4.16.** Scaling factor for interstitial insulin dependent glucose utilization

The default value of $C_3$ is 100mg/L. As $C_3$ gets larger, the function $f_3$ gets smaller. Because large values of $f_3$ correspond to faster blood glucose removal, the glucose oscillation amplitude is low for small $C_3$ since all glucose is removed as quickly as it can be added to the blood. However, if $C_3$ is large (and $f_3$ is therefore quite small), the insulin dependent utilization of glucose will cease. This is equivalent to removing the action of interstitial insulin from the model, which leads to rapid glucose saturation. Therefore, oscillations will disappear for $C_3$ higher than 200mg/L. The maximum oscillation amplitude for glucose is 35.2mg/dL when $C_3$ is 92mg/L.

### 4.3.2 Time Constants

While the time constants $t_p$, $t_i$, and $t_d$ were included in the analysis in [2], notable discrepancies exist between the values reported by Sturis et al. and those which are evident in the figures below.

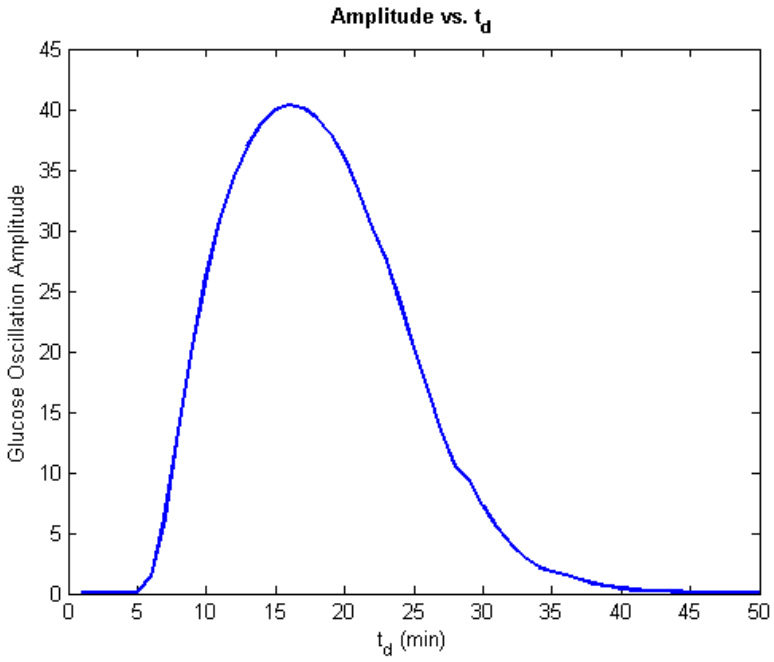


**Figure 4.17.** Linear filter time constant

In [2], $t_d$ values are three times larger than those in the figure above since the time constant is implemented in only one stage of the three-stage filter in [2], but in all three stages in this work. Therefore, in [2] Sturis et al. report oscillations from $8 \leq t_d \leq 16$. The figure above suggests that other values of $t_d$ might be equally acceptable and produce an even greater amplitude of oscillation. The maximum amplitude is achieved when $t_d$ is 16min. However, amplitudes at least as large as that when $t_d = 8$ persist with increasing $t_d$ until the parameter value is 30min.

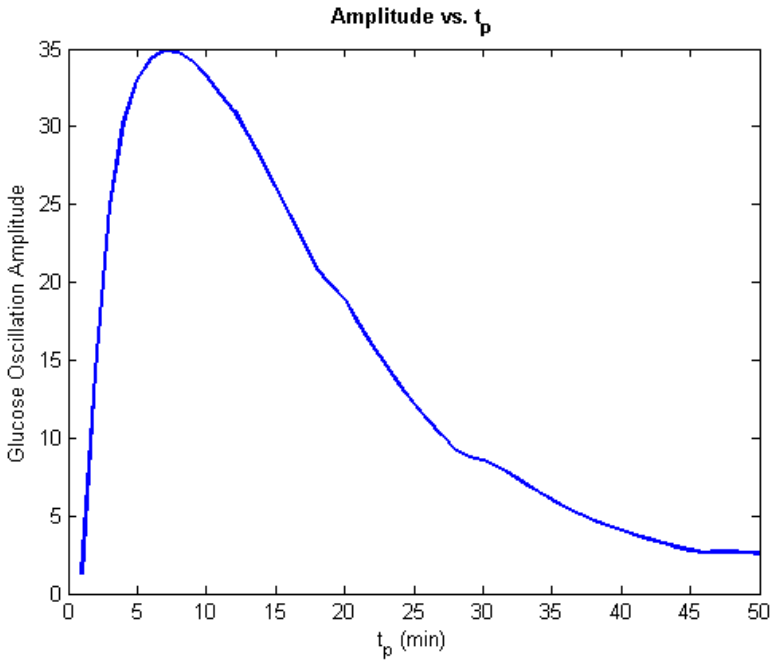


**Figure 4.18.** Spontanous decay of plasma insulin time constant

The parameter $t_p$ is the time constant for plasma insulin decay. In [2], $t_p$ is allowed to range from 4min to 8min. The figure above shows that the maximum oscillation amplitude occurs when $t_p$ is 7min. However, $t_p$ values as large as 25min produce glucose oscillations as large as those when $t_p$ is 4min.

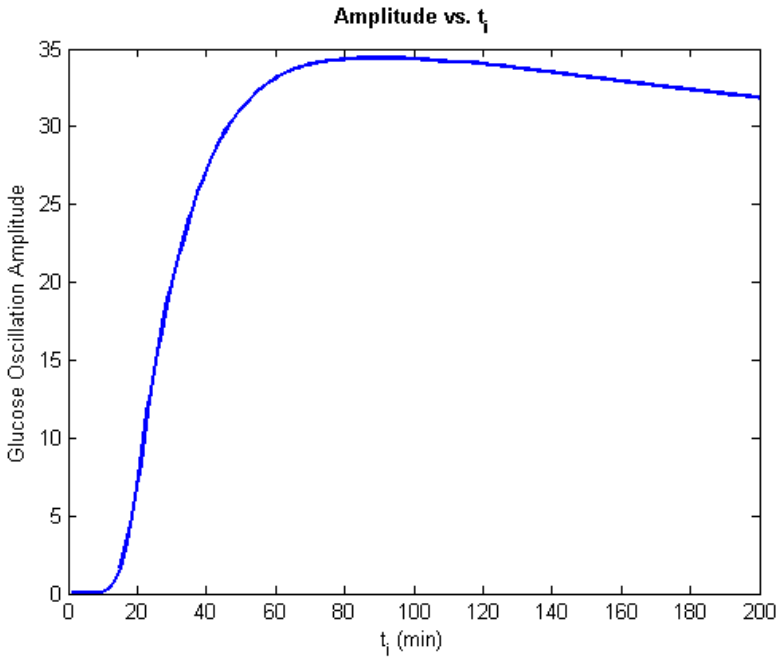


**Figure 4.19.** Spontaneous decay of interstitial insulin time constant

The parameter $t_i$ is the time constant for interstitial insulin decay. In [2], the range for this parameter is given as 60min-140min. Glucose oscillations have an amplitude of 33mg/dL when $t_i$ is 60min, and the oscillation amplitude decreases steadily after $t_i = 89min$. When $t_i$ is larger than 140min, the oscillation amplitude is less than 33mg/dL. Glucose oscillation amplitude is not highly sensitive to high $t_i$ and slow decay of interstitial insulin.

# Chapter 5
# Context 1: Continuous Glucose Monitoring in Healthy Individuals

## 5.1 Introduction

Two people, henceforth referred to as subjects 1 and 2, used Dexcom G4 Platinum sensors to record their blood glucose levels every five minutes for 39 and 31 days. Additionally, both subjects tracked all of their meals including taking photographs for evaluation by a nutritionist. This data provides a unique opportunity to study the relationship between food consumption and the dynamics of blood glucose at a high time resolution. Section 5.2 demonstrates that feeding reconstruction with from glucose measurements for this data set may yield information about feeding trends, but does not represent the amount of feeding accurately.

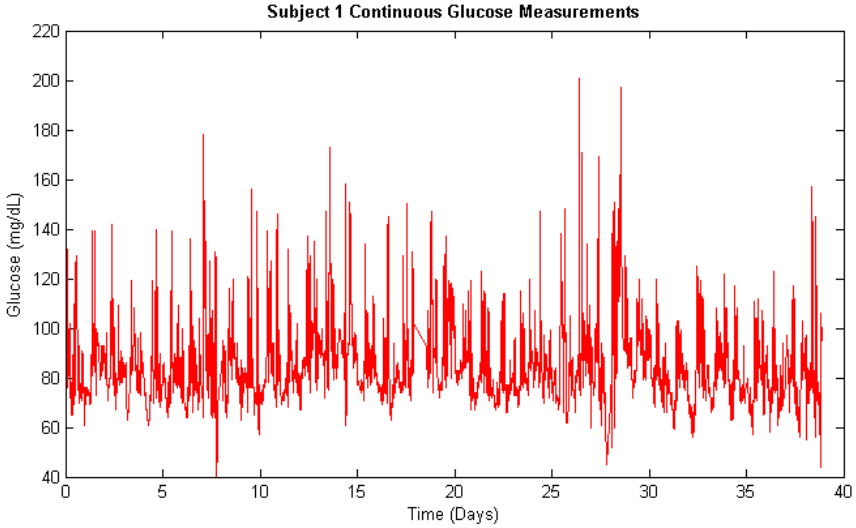


**Figure 5.1.** Subject 1 continuous blood glucose measurements

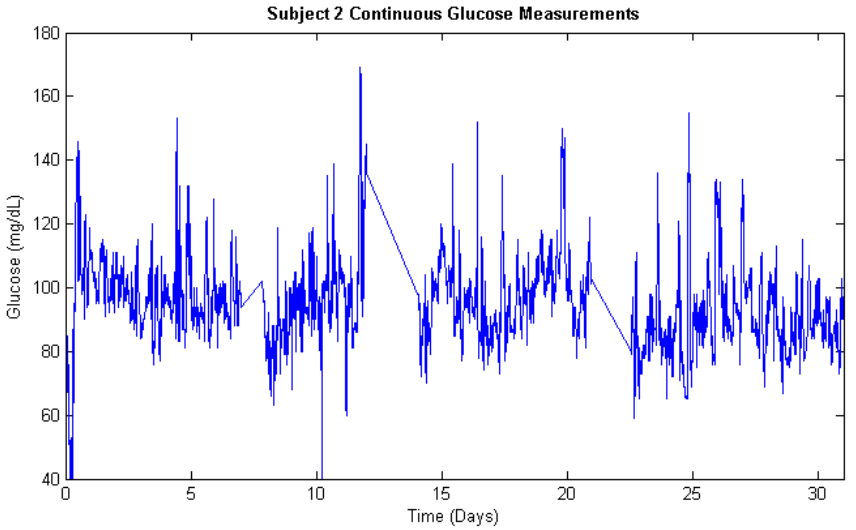


**Figure 5.2.** Subject 2 continuous blood glucose measurements

## 5.2 Feeding Reconstruction

The Unscented Kalman Filter is used with the Sturis model to reconstruct the caloric intake of subjects 1 and 2 from their continuously glucose measurements. The reconstruction does not accurately represent the quantity of feeding, although it is possible to correlate trends in the subjects' reported feeding to trends in the reconstructed feeding.

### 5.2.1 Calorie and Carbohydrate Consumption

The meals consumed by subject 1 and subject 2 were photographed and submitted for expert evaluation of calorie and carbohydrate content. Subject 1 reported 4.5 meals per day, with mean calorie and carbohydrate content of 357 calories and 29,503 mg, respectively.

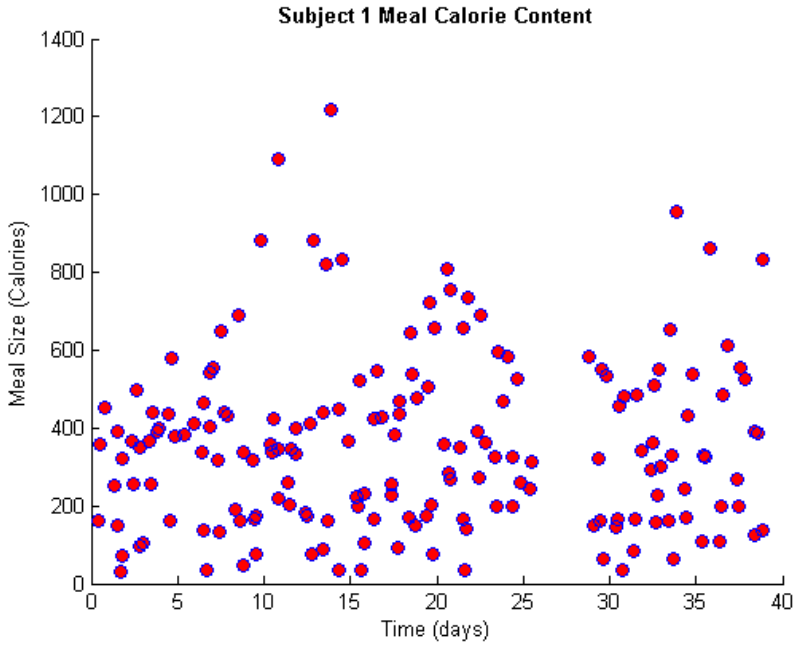


**Figure 5.3.** Subject 1 calorie consumption by meal for 39 days

Meal size ranges from 31 to 1219 calories, with a median meal size of 337 calories. The subject consumed a mean of 1602 calories in each 24-hour period, for a total of 62,493 calories over 39 days of data collection. This somewhat low number of calories consumed per day suggests a subject who is either somewhat small, a child, or on a moderately intense weight loss diet.

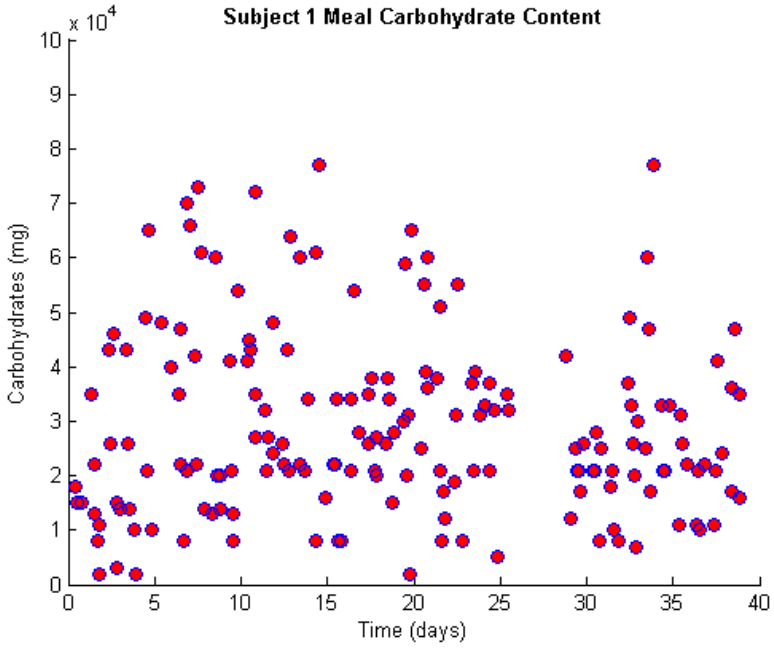


**Figure 5.4.** Subject 1 carbohydrate consumption by meal for 39 days

Subject 2 reported 2.2 meals per day, with mean calorie and carbohydrate content of 486 calories and 32,190 mg, respectively.

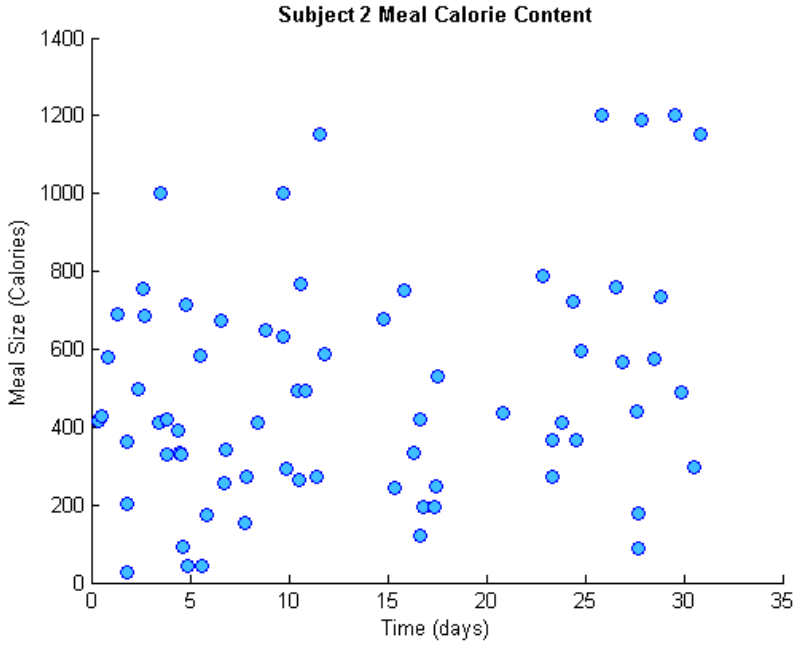


**Figure 5.5.** Subject 2 calorie consumption by meal for 31 days

Meal size ranges from 27 to 1203 calories, with a median meal size of 421 calories. The subject consumed a mean of 1069 calories in each 24-hour period, for a total of 33,139 calories over 31 days of data collection. This is a low number for most adults, and suggests that the subject was either following an extreme diet, or is a child.

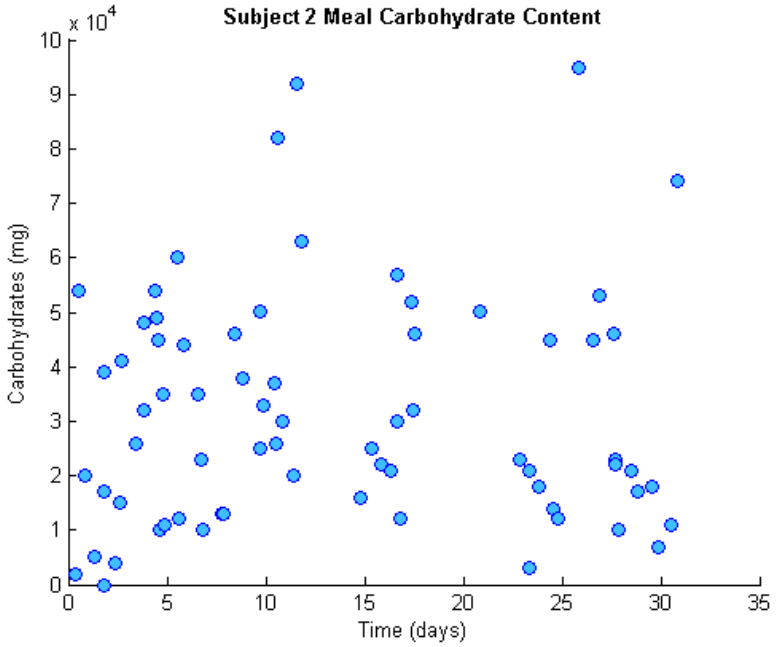


**Figure 5.6.** Subject 2 carbohydrate consumption by meal for 31 days

The distribution of carbohydrate content in the subjects' meals is similar to that of the caloric content. Since certain food types, such as protein, act much more slowly on blood glucose levels, measuring the amount of fast-acting carbohydrates consumed provides an alternative more likely to show agreement with reconstructed feeding.

### 5.2.2 Reconstructed Feeding Rate

By treating the rate of feeding as a model variable in the Unscented Kalman Filter rather than a parameter, it is possible to reconstruct the feeding rate by tracking

glucose measurements. All Sturis model parameters will remain at their default values during this simulation. One problem which may occur is the possibility of feeding taking on a negative value during precipitous declines in blood glucose. It is possible for a human being to take actions which affect dramatic change in blood glucose levels in a short amount of time. Since there is no physical analog to a negative rate of feeding, it is important to disallow this condition. Therefore, a rule is added to the Kalman Filter which states the following:

If after performing the data assimilation step of the Unscented Kalman Filter the feeding rate has become negative, set the feeding rate to zero.

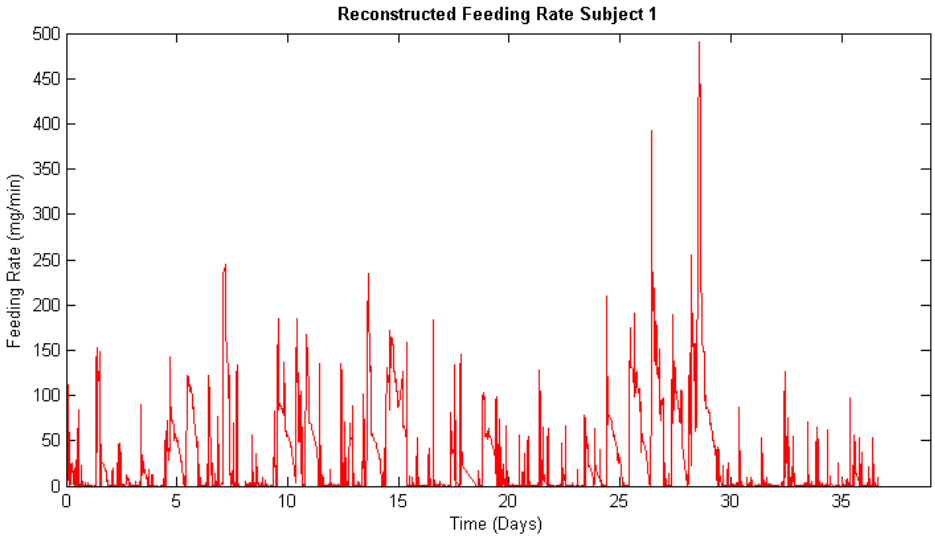


**Figure 5.7.** Subject 1 reconstructed feeding rate for 39 days

The minimum feeding rate for subject 1 is 0mg/min, and the maximum is 490.5mg/min. The mean feeding rate is 29.7mg/min. The total amount of feeding is 1,667,952mg. Since 1 calorie is roughly equal to 250mg of glucose, the total amount of feeding over all 39 days is just 6,672 calories.

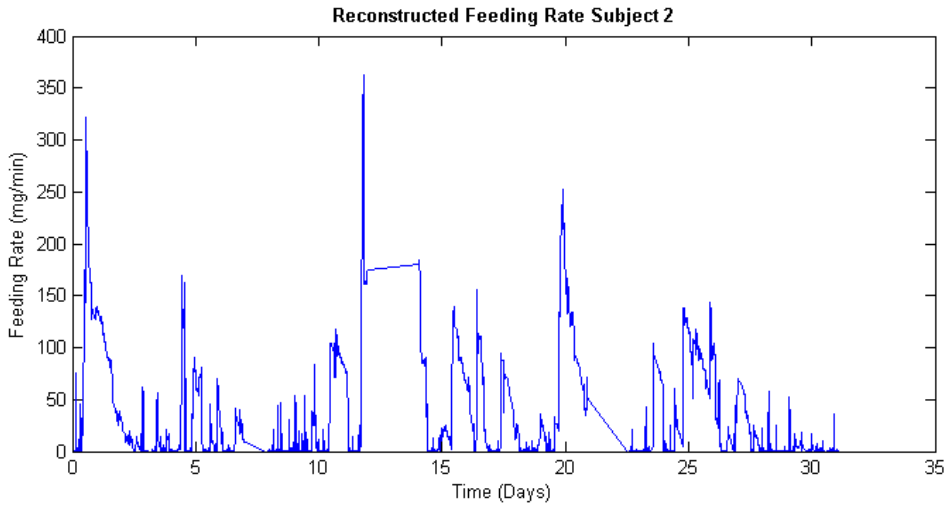


**Figure 5.8.** Subject 2 reconstructed feeding rate for 31 days

The minimum feeding rate for subject 2 is 0mg/min, and the maximum is 362.4mg/min. The mean feeding rate is 36.5mg/min. The total amount of feeding is 1,629,360mg. Since 1 calorie is roughly equal to 250mg of glucose, the total amount of feeding over all 31 days is just 6,517 calories.

The reconstructed total calorie estimates of 6,672 calories and 6,517 calories for subjects 1 and 2 are not close to the 62,493 and 33,139 calorie totals which they reported. Such a large discrepancy might be explained by a few factors. First, not all calories consumed will be digested by the body. Second, it is possible that the Sturis model parameters used in this model are not well-suited to subjects.

The shape of the reconstructed feeding curve has some properties which suggest it is correlated to actual feeding rate. When the subject consumes a meal, their blood glucose will rise quickly as sugars and carbohydrates are quickly digested. Then, the feeding rate will gradually decline as these fast burning foods are depleted. Protein and other food types may continue to maintain a small, declining feeding rate for hours or minutes more. Between meals, the feeding rate will eventually fall to zero. In the reconstructed feeding curve, a baseline of zero feeding is interspersed with high peaks. These peaks represent a rapid rise in the feeding rate, followed

by a gradual decline. Although the magnitude of the reconstructed feeding rate is far too small, the shape of the curve suggests the expected feeding rate dynamics around meal times.

There is a gap in glucose measurements from 11.98 - 14.04 days while the subject was not wearing their glucose sensor. Data on both sides of this gap must be treated separately, as the rate of feeding leading up to it is not related to the rate of feeding once data collection resumes. Another gap is present beginning on day 22.

The region from day 15 to day 21 is free from sensor cleaning interruptions, and contains reconstructed curves which resemble digestion of a meal. Let us choose this region for more detailed investigation.

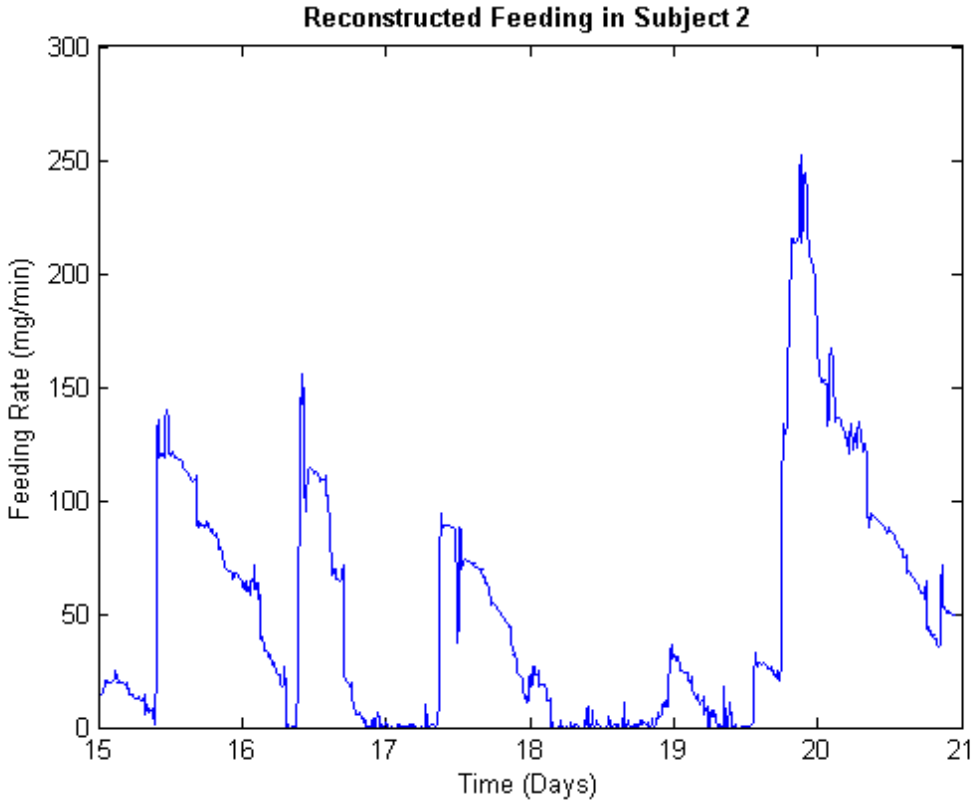


**Figure 5.9.** Subject 2 reconstructed feeding days 15-21

The reconstructed feeding rate is not of high enough magnitude to accurately represent the calories which subject 2 consumed. However, by integrating the reconstructed feeding function between meals it is possible to determine whether the reconstructed feeding captures the overall trend in feeding.

Subject 2 consumed 2 or 3 meals on each of the days from day 15 to day 21. Integrating between mealtimes and summing all meals consumed on the same day. This calculation will yield a reconstructed estimate of the number of calories consumed on each day from day 15 to day 21 which can be compared to the reported calories consumed on these days.

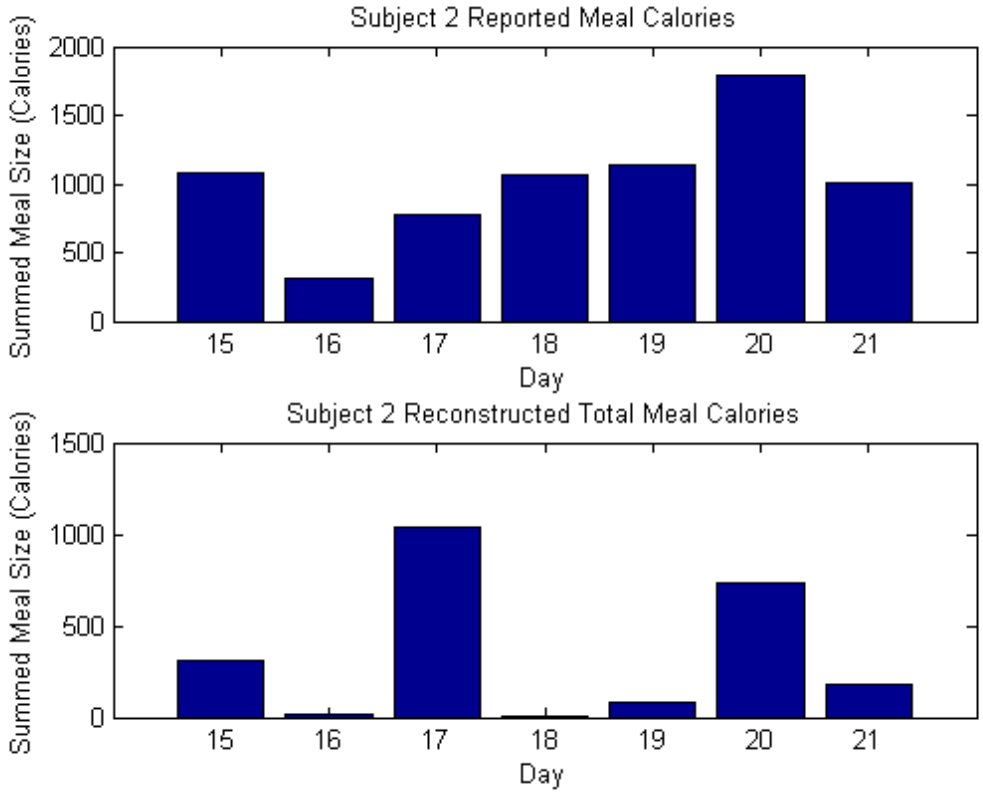


**Figure 5.10.** Subject 2 actual vs. reconstructed total calories days 15-21

Except on day 17, the reconstructed calorie total is lower for each day than the real number of calories consumed. Excepting day 17, the overall trend in feeding from day to day is reflected in the reconstructed feeding. One possible explanation for the large magnitude of the reconstructed feeding on day 17 compared to other days is that they consumed a small meal (195 calories) that contained a high amount of carbohydrates (52000mg). To investigate the relationship between carbohydrates and the reconstructed feeding, the analysis from days 15-21 is repeated below using daily carbohydrate totals rather than calorie totals.

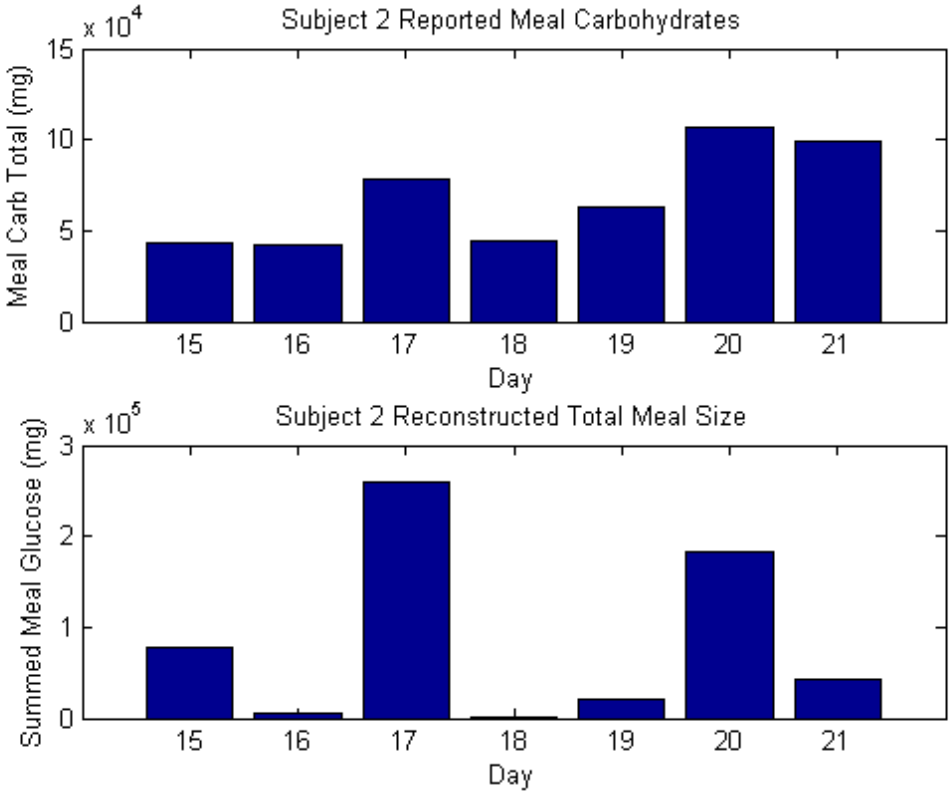


**Figure 5.11.** Subject 2 actual vs. reconstructed total carbohydrates days 15-21

While the reconstructed carbohydrate total for day 17 is still very high, the trend in true carbohydrate consumption matches the trend in the reconstructed carbohydrate total for each day.

### 5.2.3 Summary

Reconstruction of the caloric intake from measurements of glucose would serve as a validation of the Sturis model's representation of glucose/insulin dynamics. While successful reconstruction might increase our confidence that the Sturis model is useful in predicting future glucose behavior, failed reconstruction decreases this confidence.

Reconstruction of feeding from glucose measurements with the Unscented Kalman Filter as performed in this chapter was unsuccessful at approximating the caloric intake of both subjects. There are several reasons:

1. The rate of feeding input varies greatly depending on the type and quantity of food consumed. If this is true, mapping food type and quantity to patterns in the feeding rate is an important next step in enabling accurate feeding reconstruction. This theory is supported by the fact that carbohydrate appears to correlate more strongly with reconstructed feeding rate than raw calories.

2. In addition to assuming that the Sturis model is an accurate representation of glucose/insulin dynamics, this analysis used the parameter values presented in [2]. Many parameters from the Sturis model are correlated to physical, anatomical traits such as total blood volume, or total interstitial tissue volume.

At best, the feeding reconstructions for subjects 1 and 2 accurately represent the overall trend in the rate of feeding over time. However, the total caloric consumption represented by reconstructed feeding is not close to reported calories consumed. Parameter fitting for individual subjects might yield better feeding reconstructions.

# Chapter 6
# Context 2: Comatose Patients in the Neuro-ICU

## 6.1 Introduction

Comatose patients rely on glucose feeding tubes to maintain acceptable levels of blood glucose. Anonymized patient data from the Electronic Health Record provides an opportunity to study glucose/insulin dynamics with constant feeding rates. In section 6.2, the rate of feeding is reconstructed for three comatose Neuro-ICU patients using sparse measurements of blood glucose. The feeding reconstruction demonstrates clear correlation with the real rate of feeding, but tends to fail when there is a cusp in the rate of feeding. Large increases or decreases in the rate of feeding may decrease the efficacy of the feeding reconstruction.

## 6.2 Feeding Reconstruction

The Unscented Kalman Filter is used with the Sturis model to reconstruct the feeding rate of several patients from the Electronic Health Record dataset. The feeding reconstructions demonstrate some agreement with reported feeding rates, but can wander off track when the feeding rate is lowered to zero.

### 6.2.1 Patient Selection and Glucose Levels

The quality of data varies greatly in the Electronic Health Record glucose and feeding dataset. Some patients have glucose measurements reported as often as each hour, while others are only measured once a day or less. Feeding rate adjustments may happen multiple times per hour, or never. Several properties of patient data are desirable for attempts to reconstruct the feeding function:

1. Glucose measurement frequency should be high
2. Feeding rate should be constant or simple, without to many adjustments

Based upon these criteria, three subsets of data were selected from a dataset with 599 patients to choose from. The subsets each comes from a different patient, and will be referred to with the number of the patient from the original dataset. The datasets are:

- The first 12 days of data for patient 219
- The first 14 days of data for patient 311
- The first 18 days of data for patient 354

Data selection was made with a focus on identifying large numbers of glucose measurements to use in reconstructing the feeding function.

The patient data excerpts in the figures below contain 161, 143, and 169 glucose measurements. While the measurement frequency does not approach that of the continuous glucose monitoring dataset, these patients had their glucose recorded often enough that oscillations are apparent.

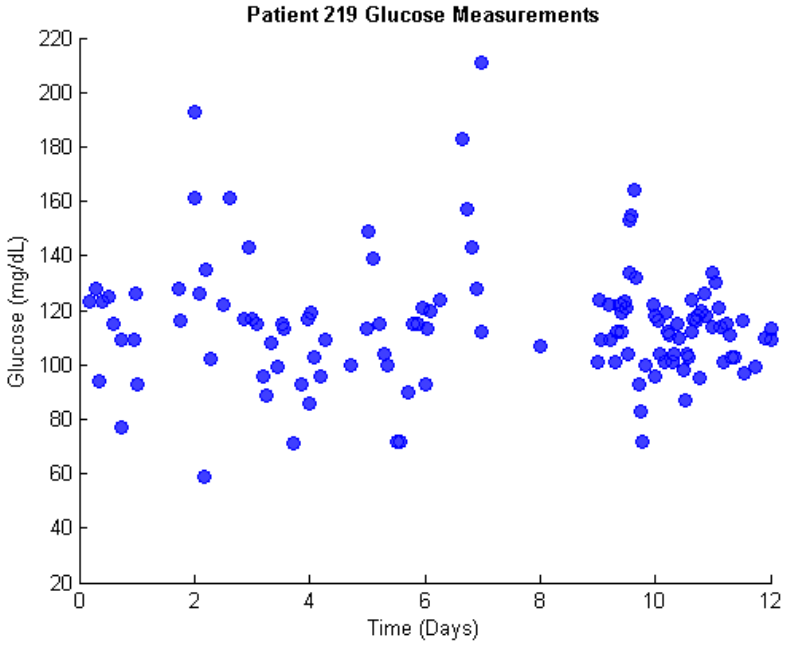


**Figure 6.1.** Glucose measurements from patient 219

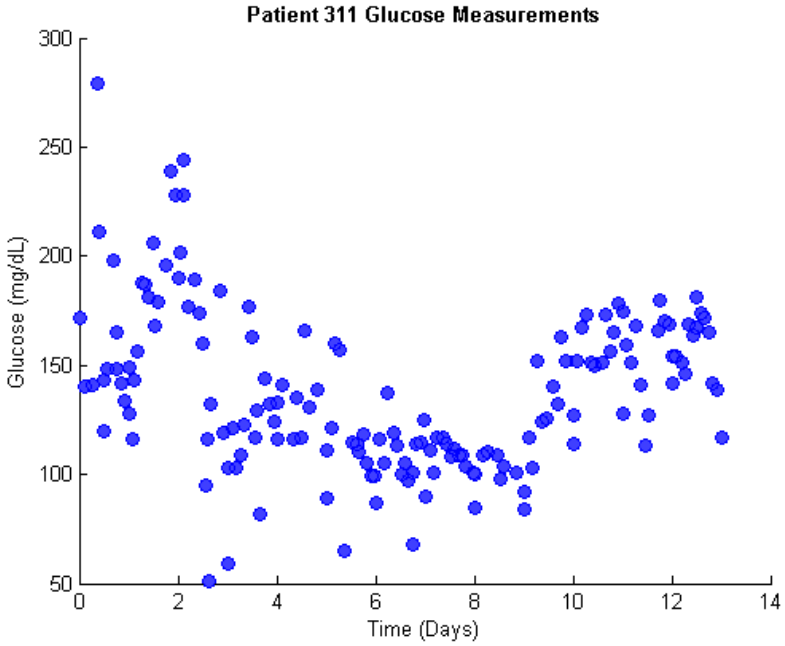


**Figure 6.2.** Glucose measurements from patient 311

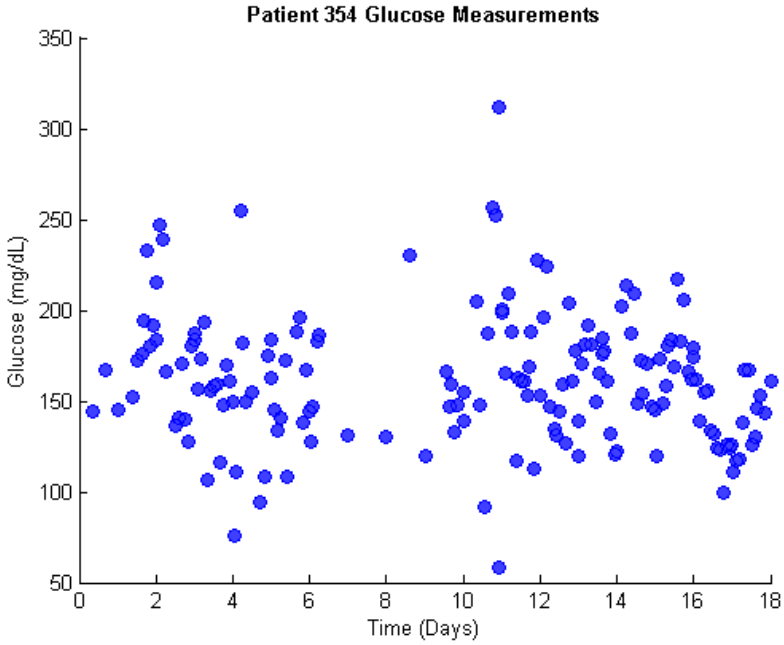


**Figure 6.3.** Glucose measurements from patient 354

### 6.2.2 Reconstructed Feeding Rate

Although the data in this section is sparse compared to the glucose data from chapter 5, the feeding behavior is dramatically simplified. The selected portions of data do not have constant rates of feeding throughout, but also do not generally have multiple adjustments within at least an hour.

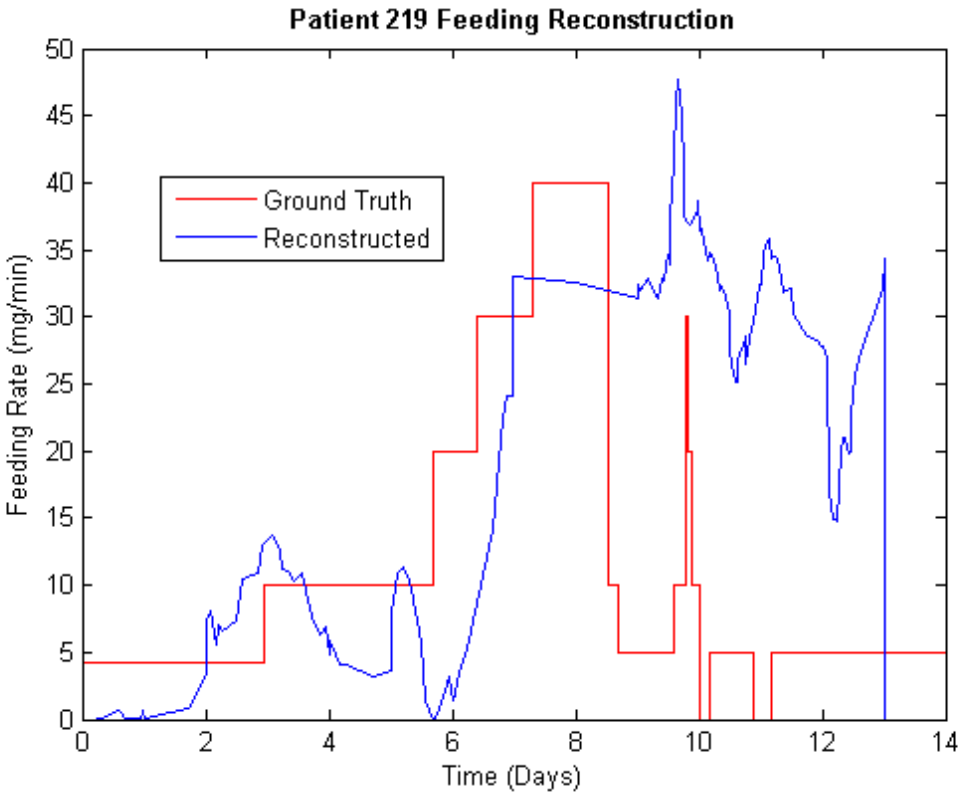


**Figure 6.4.** Patient 219 Feeding Reconstruction

From day 1 to day 8, the feeding rate reconstruction is fairly accurate. Although it wanders, it typically remains within $\pm$10mg/min of the ground truth feeding rate. However, once the feeding rate is decreased dramatically on the 8th day, the feeding reconstruction does not recover.

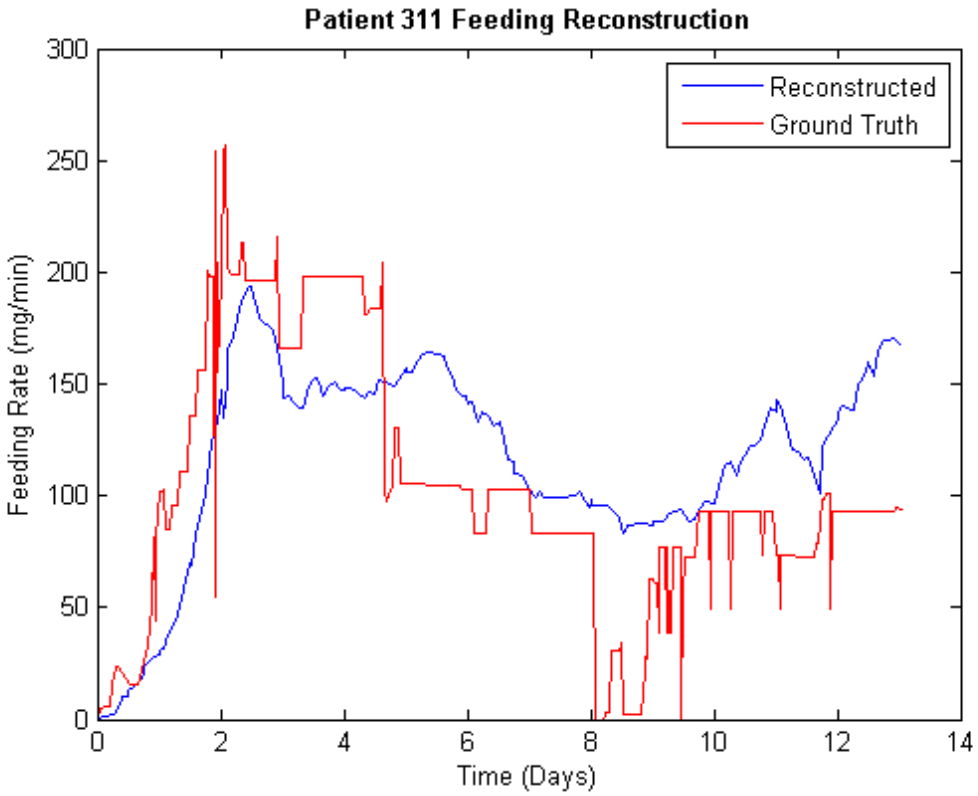


**Figure 6.5.** Patient 311 feeding reconstruction

Despite the fact that the ground truth feeding rate is adjusted multiple times per day, the reconstructed feeding rate appears to convincingly follow the trend of the ground truth feeding. After the sudden decrease in the feeding rate on the 4th day, the reconstructed feeding begins to recover. Like for the feeding reconstruction from patient 219, dramatic and sudden decreases in the feeding rate seem to cause the feeding reconstruction to wander.

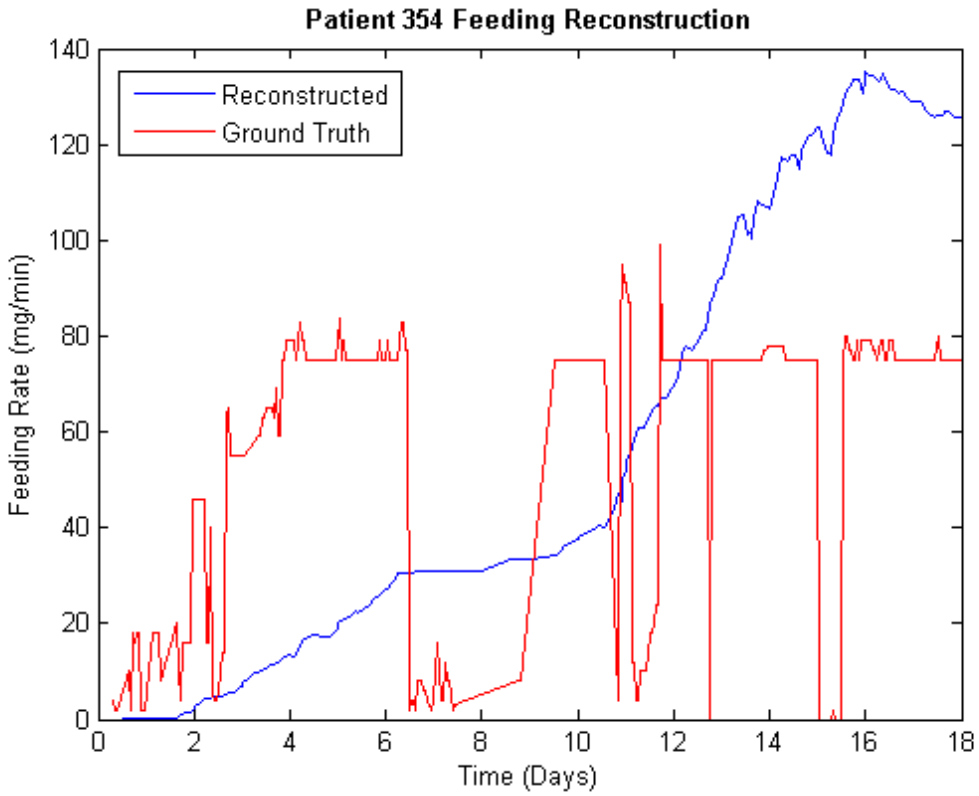


**Figure 6.6.** Patient 354 feeding reconstruction

The feeding reconstruction for patient 354 fails. One reason that this data is particularly challenging is that the ground truth feeding rate is adjusted constantly and by large amounts. The feeding rate is intermittently reduced to low values between 10-20 mg/min, before being raised back to 76mg/min. The sharp changes in the feeding rate create a situation which feeding reconstruction is not well-suited to track.

Even though glucose measurements are only available in patients 219, 311, and 354 on a less than hourly basis, feeding reconstruction was moderately successful on two of these datasets. Characteristics of data that are good candidates for feeding reconstruction:

1. Smooth transitions between different feeding rates

2. Infrequent adjustment to the feeding rate

3. High number of glucose measurements available for data assimilation

Feeding reconstruction was somewhat successful for glucose datasets from comatose Neuro-ICU patients. This technique has potential when the feeding rate is known to be constant, and a relatively high frequency of glucose measurement is possible.

# Chapter 7
# Conclusion

## 7.1 Contribution

This work constitutes the first attempt known to the author to retroactively estimate food consumption using measurements of blood glucose levels. Parameter characterization of the Sturis model in chapter 4 provides new insight about the sensitivity of ultradian glucose and insulin oscillations to physically meaningful parameters such as the rate of glucose utilization by the brain ($U_b$) and the rate of insulin production in response to rising blood glucose ($R_m$). Chapter 4's characterization of oscillatory sensitivity to seven different parameters extends work which was presented in [2], leveraging the increased processing power of modern computers to perform a more exhaustive analysis than was feasible at the time of the original publication of the Sturis model. Reconstruction of the feeding function in subjects with continuous glucose monitoring showed that the potential exists to map reconstructed feeding to trends in caloric intake. Feeding reconstruction in Electronic Health Record data from comatose patients showed that the Sturis model has great potential in the estimation of feeding rate magnitude. Several data characteristics were identified which are likely to present a challenge to accurate feeding reconstruction, such as large and instantaneous changes in the rate of feeding.

## 7.2 Future Work

Certain parameter values in the Sturis model represent implicit assumptions about specific elements of physiology such as total blood volume, and volume of interstitial tissue. Subjects 1 and 2 from chapter 5 consumed an average of 1602 and 1069 calories each day, respectively. Their low caloric intake implies a non-standard adult body type. This means that many of the default parameter values from [2] may not apply to subjects 1 and 2. One way to improve the accuracy of feeding reconstruction is to perform parameter fitting such that the default values from the Sturis model might converge on more appropriate values for subjects 1 and 2.

The feeding reconstructions from chapter 6 show great promise for future effort on the Electronic Health Record dataset. An important step will be to fully characterize conditions which lead to poor feeding rate reconstruction. If it is possible to predict when these conditions exist, then confidence in feeding reconstruction can be measured at different points. This may eventually lead to the ability to correct for standard types of reconstruction errors automatically, effectively increasing the accuracy of the technique. Reconstruction of feeding for this dataset may also benefit from parameter fitting.

# Bibliography


[1] Berger, M. and D. Rodbard (1989) "Computer Simulation of Plasma Insulin and Glucose Dynamics After Subcutaneous Insulin Injection," *Diabetes Care*, **12**(10), pp. 725–736.

[2] Sturis, J., K. S. Polonsky, E. Mosekilde, and E. Van Cauter (1991) "Computer model for mechanisms underlying ultradian oscillations of insulin and glucose," *American Journal of Physiology*, pp. 801–809.

[3] Keener, J. P. and J. Sneyd (2009) *Mathematical physiology*, Springer.

[4] Sedigh-Sarvestani, M., D. J. Albers, and B. J. Gluckman (2012) "Data assimilation of glucose dynamics for use in the intensive care unit," *2012 Annual International Conference of the IEEE Engineering in Medicine and Biology Society*.

[5] Miller, M. (2016) *State estimation of glucose and insulin dynamics*, Master's thesis, Cleveland University.
URL `http://engagedscholarship.csuohio.edu/etdarchive/925/`

[6] Han, K., H. Kang, M. Choi, J. Kim, and M.-S. Lee (2012) "Mathematical model of the glucose-insulin regulatory system: From the bursting electrical activity in pancreatic $\beta$-cells to the glucose dynamics in the whole body," *Physics Letters A*, **376**(45), pp. 3150–3157.

[7] Terejanu, G. A., "Unscented Kalman Filter Tutorial," .
URL `https://cse.sc.edu/ terejanu/files/tutorialUKF.pdf`

[8] Clark, P. M. S. and C. N. Hales (1994) "How to measure plasma insulin," *Diabetes / Metabolism Reviews*, **10**(2), pp. 79–90.

[9] Bergman, R. N. (1989) "Toward Physiological Understanding of Glucose Tolerance: Minimal-Model Approach," *Diabetes*, **38**(12), pp. 1512–1527.

[10] Albers, D. J., G. Hripcsak, and M. Schmidt (2012) "Population Physiology: Leveraging Electronic Health Record Data to Understand Human Endocrine Dynamics," *PLoS ONE*, **7**(12).

[11] Boiroux, D., T. B. Aradottir, M. Hagdrup, N. K. Poulsen, H. Madsen, and J. B. Jorgensen (2015) "A Bolus Calculator Based on Continuous-Discrete Unscented Kalman Filtering for Type 1 Diabetics: Funded by the Danish Diabetes Academy supported by the Novo Nordisk Foundation. Contact information: John Bagterp Jorgensen (jbjo@dtu.dk)." *IFAC-PapersOnLine*, **48**(20), pp. 159–164.

[12] Gough, D. A., K. Kreutz-Delgado, and T. M. Bremer (2002) "Frequency Characterization of Blood Glucose Dynamics," *Annals of Biomedical Engineering*, **31**(1), pp. 91–97.

[13] J.-L. Chen and, H.-M. W., P.-F. Chen and) (2014) "Decreased complexity of glucose dynamics in diabetes: evidence from multiscale entropy analysis of continuous glucose monitoring system data," *AJP: Regulatory, Integrative and Comparative Physiology*, **307**(2).

[14] Tirosh, A., I. Shai, D. Tekes-Manova, E. Israeli, D. Pereg, T. Shochat, I. Kochba, and A. Rudich "Normal Fasting Plasma Glucose Levels and Type 2 Diabetes in Young Men," *The New England Journal of Medicine*, **353**(14), pp. 1454–1462.

# KENNETH T. HALL

Phone: (240) 586-1036 | Email: kthall.2013@gmail.com

## EDUCATION

**The Pennsylvania State University**, University Park, PA
College of Engineering, Schreyer Honors College
Major: Engineering Science
Graduation May 2017

## EXPERIENCE

**Undergraduate Research Assistant** *May 2016 - Present*
**Applied Research Laboratory** *University Park, PA*

- Implemented real-time object detection, recognition, and tracking system with OpenCV, Dlib, C++.
- Ongoing Work: Design neural networks with Tensorflow to perform tasks such as classification with online learning.

**Undergraduate Research Assistant** *Jan 2016 - Present*
**Penn State Center for Neural Engineering** *University Park, PA*

- Use data assimilation techniques to fit a mathematical model of glucose/insulin dynamics to Electronic Health Record data from comatose patients.
- Thesis: Data Assimilation of Glucose Dynamics for the Neuro-ICU, under the supervision of Dr. Bruce Gluckman.

**Undergraduate Teaching Assistant** *Aug 2016 - Dec 2016*
**Penn State College of Engineering** *University Park, PA*

- Teach and tutor students in Penn State's award-winning Engineering Design 100H class with Professor Matt Parkinson.
- Contributed to reverse-engineering project for teaching CAD.

**Intern** *June 2012 - Aug 2014*
**National Cancer Institute** *Fort Detrick, MD*

- Implemented Anisotropic Network Models and Molecular Dynamics simulations for engineered RNA polygons and cubes.
- Mentored four interns (summer 2013, 2014) in Bash, C, C++, Perl.

## SKILLS

| | |
|---|---|
| Languages | Bash, MATLAB, C++, Perl, Python, *Mathematica*, PHP |
| Frameworks | Tensorflow, OpenCV, SolidWorks, Unity, PyMOL |
| Systems | Linux (Red Hat, Ubuntu, Mint), OSX, Windows |

## PUBLICATION

Afonin, Kirill A., Wojciech Kasprzak, Eckart Bindewald, Praneet S. Puppala, Alex R.Diehl, **Kenneth T. Hall**, Tae Jin Kim, Michael T. Zimmermann, Robert L. Jernigan, Luc Jaeger, and Bruce A. Shapiro. "Computational and Experimental Characterization of RNA Cubic Nanoscaffolds."*Methods* (2013)